



Structural optimization of 4-(imidazol-5-yl)pyridine derivatives affords broad-spectrum anticancer agents with selective B-RAF^{V600E}/p38 α kinase inhibitory activity: Synthesis, *in vitro* assays and *in silico* study

Eslam M.H. Ali^{a,b,c}, Karim I. Mersal^{a,b,c}, Usama M. Ammar^d, Seyed-Omar Zareai^{a,b}, Mohammed S. Abdel-Maksoud^e, Mohammed I. El-Gamal^{f,g,h}, Md Mamunul Haqueⁱ, Tanuza Das^j, Eunice EunKyeong Kim^j, Jun-Seok Leeⁱ, Kwan Hyi Lee^{a,k}, Hee-Kwon Kim^{l,m,*}, Chang-Hyun Oh^{a,b,*}

^a Center of Biomaterials, Korea Institute of Science & Technology (KIST School), Seoul, Seongbuk-gu, 02792, Republic of Korea

^b University of Science & Technology (UST), Daejeon, Yuseong-gu, 34113, Republic of Korea

^c Pharmaceutical Chemistry Department, Faculty of Pharmacy, Modern University for Technology and Information (MTI), Cairo, 12055, Egypt

^d Strathclyde Institute of Pharmacy and Biomedical Sciences, University of Strathclyde, 161 Cathedral Street, Glasgow G4 0NR, Scotland, United Kingdom

^e Medicinal & Pharmaceutical Chemistry Department, Pharmaceutical and Drug Industries Research Division, National Research Centre NRC (ID: 60014618)), Dokki, Giza, 12622, Egypt

^f Department of Medicinal Chemistry, College of Pharmacy, University of Sharjah, Sharjah, 27272, United Arab Emirates

^g Sharjah Institute for Medical Research, University of Sharjah, Sharjah, 27272, United Arab Emirates

^h Department of Medicinal Chemistry, Faculty of Pharmacy, Mansoura University, Mansoura 35516, Egypt

ⁱ Department of Pharmacology, College of Medicine, Korea University, Seoul 02841, Republic of Korea

^j Biomedical Research Institute, Korea Institute of Science and Technology, Seoul 02792, Republic of Korea

^k KU-KIST Graduate School of Converging Science and Technology, Korea University, Seoul 02841, Republic of Korea

^l Department of Nuclear Medicine, Molecular Imaging & Therapeutic Medicine Research Center, Jeonbuk National University Medical School and Hospital, 20 Geonji-ro, Deokjin-gu, Jeonju 54907, Republic of Korea

^m Research Institute of Clinical Medicine of Jeonbuk National University-Biomedical Research Institute of Jeonbuk National University Hospital, 20 Geonji-ro, Deokjin-gu, Jeonju 54907, Republic of Korea

ARTICLE INFO

Keywords:

Anticancer
Imidazolylpyridine
B-RAF^{V600E}
p38 α
Cell cycle arrest
Molecular modeling

ABSTRACT

In the current article, we introduce design of a new series of 4-(imidazol-5-yl)pyridines with improved anticancer activity and selective B-RAF^{V600E}/p38 α kinase inhibitory activity. Based on a previous work, a group of structural modifications were applied affording the new potential antiproliferative agents. Towards extensive biological assessment of the target compounds, an *in vitro* anticancer assay was conducted over NCI 60-cancer cell lines panel representing blood, lung, colon, CNS, skin, ovary, renal, prostate, and breast cancers. Compounds **7c**, **7d**, **8b**, **9b**, **9c**, **10c**, **10d**, and **11b** exhibited the highest potency among the tested compounds and demonstrated sub-micromolar or one-digit micromolar GI₅₀ values against the majority of the employed cell lines. Compound **10c** emerged as the most potent agent with nano-molar activity over most of the cells and incredible activity against melanoma (MDA-MB-435) cell line (GI₅₀ 70 nM). It is much more potent than sorafenib, the clinically used anticancer drug, against almost all the NCI-60 cell lines. Further cell-based mechanistic assays showed that compound **10c** induced cell cycle arrest and promoted apoptosis in K562, MCF-7 and HT29 cancer cell lines. In addition, compound **10c** induced autophagy in the three cancer cell lines. Kinase profiling of **10c** showed its inhibitory effects and selectivity towards B-RAF^{V600E} and p38 α kinases with IC₅₀ values of 1.84 and 0.726 μ M, respectively. Docking of compound **10c** disclosed its high affinity in the kinases pockets. Compound **10c** represent a promising anticancer agent, that could be optimized in order to improve its kinase activity aiming at developing potential anticancer agents. The conformational stability of compound **10c** in the active site of B-RAF^{V600E} and p38 α kinases was studied by applying molecular dynamic simulation of the compound in the two kinases for 600 ns in comparison to the native ligands.

* Corresponding authors:

E-mail addresses: hkkim717@jbnu.ac.kr (H.-K. Kim), choh@kist.re.kr (C.-H. Oh).

<https://doi.org/10.1016/j.ejps.2022.106115>

Received 29 September 2021; Received in revised form 26 November 2021; Accepted 17 December 2021

Available online 4 January 2022

0928-0987/© 2022 The Authors.

Published by Elsevier B.V. This is an open access article under the CC BY-NC-ND license

(<http://creativecommons.org/licenses/by-nc-nd/4.0/>).

1. Introduction

Cancer is a major public health problem worldwide and is considered the second leading cause of death after cardiac diseases (Krishnan et al., 2020). In 2019, the World Health Organization (WHO) estimated that cancer is the first or second foremost cause of death before the age of 70 years in 112 of 183 countries and ranks third or fourth in a further 23 countries (Mathers, 2020). Despite the diversity of cancer treatment strategies, chemotherapy has been the most common approach for cancer therapy (Chabner and Roberts, 2005). Up to date, over 100 anticancer agents have been approved by U.S. Food and Drug Administration (FDA) (Wan et al., 2019). The currently available chemotherapeutics are widely used and exhibit a remarkable result in the treatment of various cancer types. However, chemotherapies are hampered by their low specificity and the consequent undesirable side effects and toxicity (Zhang et al., 2019). In addition, the arisen drug resistance occurs to be the major obstacle for the success cancer chemotherapy plans and even the most effective therapy usually fails to bring a complete and lasting tumor cure (Chatterjee and Bivona, 2019, Garcia-Mayea et al., 2020). Therefore, developing new anticancer agents with improved potency, low toxicity, and multiple mechanisms of action represents a challenge for pharmaceutical researchers (Bolognesi and Cavalli, 2016, Ding et al., 2020). Targeting protein kinases is one of the most common and efficient strategy in cancer therapy because of their crucial rule in mediating most cellular signal transductions and regulate different vital cellular activities such as proliferation, survival, apoptosis, metabolism, transcription, differentiation, and a wide array of other cellular process (Wada and Penninger, 2004, Shchemelinin et al., 2006). Mitogen-activated protein kinases (MAPKs) are key regulators in transduction of extracellular stimuli to cellular responses (Aouadi et al., 2006). MAPKs consist of three main families: ERKs (extracellular-signal-regulated kinases), JNKs (c-Jun N-terminal kinases), and p38/SAPKs (stress-activated protein kinases) (Zhang and Dong, 2007). RAF kinases (ARAF, BRAF, and CRAF) embrace key components in ERK branch of MAPK cascade. RAF kinases bind to RAS as the upstream activator and this results in consequent activation of both MEK 1/2 and their downstream regulators ERK1/2, which finally leads to promotion of cell proliferation and migration (Kidgera et al., 2017, Roskoski Jr, 2019). BRAF mutation is detected in 60% of melanoma and in a number of human cancer types such as colorectal

carcinomas, papillary thyroid carcinoma, hairy cell leukemia, and lung cancer (Corcoran et al., 2010, Tiacchi et al., 2011, Prahallad et al., 2012, Holderfield et al., 2014). On other hand, p38 MAPKs isoforms (p38 α , β , γ , and δ) are activated in response to stress or cytokines. MAP3K phosphorylates either MKK3 or MKK6, that then phosphorylates the activation loop of p38 isoforms, which consequently activate various p38 MAPK substrates like transcription factors, protein kinases as well as other proteins such as Cdc25 and GS, that leads finally to regulation of cell migration, invasion, and metastasis (Ono and Han, 2000, Cuenda and Rousseau, 2007, El Rawas et al., 2020). Furthermore, p38 α regulates the tumor suppressor protein, which mediates apoptotic cell death (Düzgün et al., 2017, Amin et al., 2018). Developing BRAF inhibitors and p38 α inhibitors is considered a successful strategy for the treatment of MAPK pathway hyperactivation-related disorders.

In our previous work, we reported the design and synthesis of pyridinyl imidazole and pyrimidinyl imidazole derivatives as potent, dual inhibitors of BRAF^{V600E} and p38 α kinases (Ali et al., 2021a, Ali et al., 2021b, Ali et al., 2021c). The reported compounds exhibited distinguished inhibitory activity against BRAF^{V600E} and p38 α kinases (IC₅₀ values of 2.5 and 85 nM, respectively) for the most potent derivative (Ali et al., 2021c). Despite their high potency against kinases, those previously reported derivatives did not exhibit promising anticancer activity, which could be owing to poor cell permeability. For example, the most potent kinase inhibitor of the previously reported series demonstrated modest potency against LOX IMVI melanoma cell line (IC₅₀ = 13.9 μ M, Fig. 1). In the current study, a group of structural optimizations were conducted aiming at improving the compound's lipophilicity and their cell permeability along with maintaining their enzyme inhibitory activity. As illustrated in Fig. 1, the modifications targeted two sites. The first is the substitution at imidazole's C2, which represents either the water accessible area in BRAF kinase or the phosphate binding region in p38 α kinase. In the previous work, C2 was substituted by phenyl moiety, which did not show a significant contribution to the compound's affinity to the active site of the two kinases. In the present work, different hydrophilic substituents (amides, sulfonamides, and carbamates) were introduced in this position striving for enhancing either the compounds solubilization in the BRAF kinase or enabling the compounds extension in the phosphate area of p38 α . The second presented modification was targeting the substitution at C5 of the imidazole ring, which is hypothesized to either contribute in the BRAF inhibitors

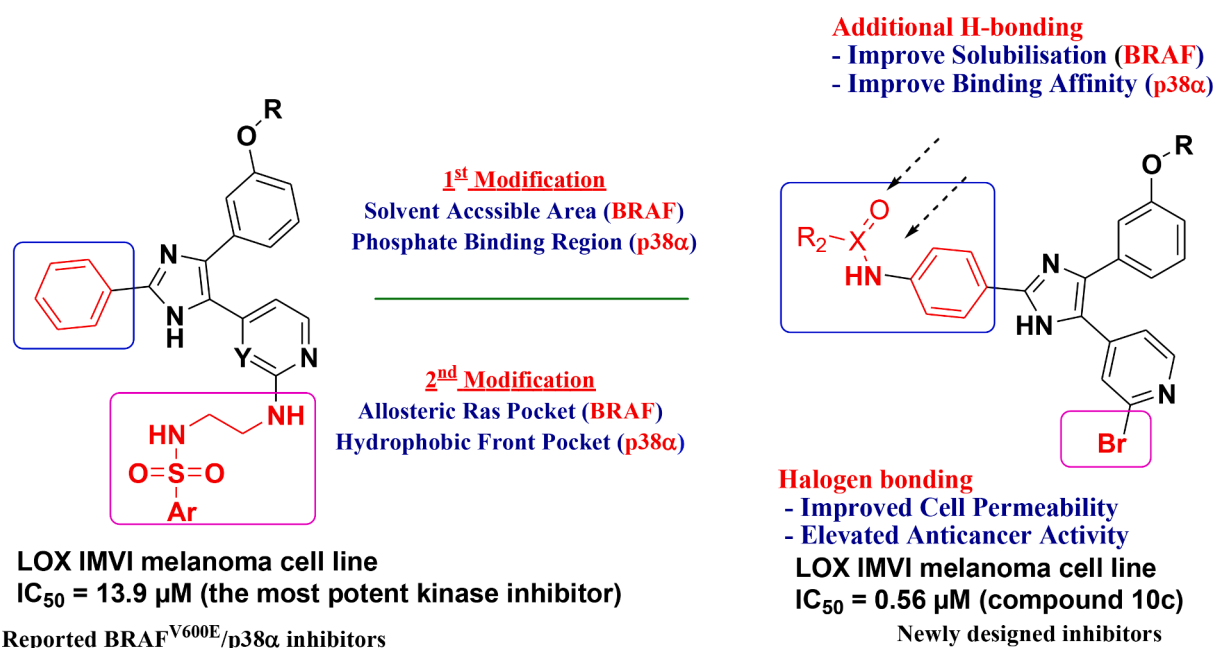


Fig. 1. Structural optimization of reported imidazole derivatives to afford new derivatives with improved binding affinity and antiproliferative activity.

unique binding in the RAS pocket or provide extra binding in p38 α front pocket. In the current work, structural simplification occurred by replacement of the long chain substitutions on the pyridine ring with bromine atom, which is proposed to form a halogen bond in the two kinases active sites, as well as improving the cell permeability.

Herein, we present the development of 4-(imidazol-5-yl)pyridine-based derivatives with highly improved broad-spectrum anticancer activity. The anticancer activity of target compounds was evaluated over NCI-60 human cancer cell lines panel. After preliminary testing of the target compounds at 10 μ M concentration, eight compounds were further evaluated in 5-dose assay to determine their IC₅₀ values. It demonstrated an extraordinary potency against the NCI-60 cell line panel. Most of its IC₅₀ values are in sub-micromolar scale, and it is much more potent than sorafenib, reference standard anticancer drug. *In vitro* cell-based mechanistic studies and autophagy analysis were conducted for the most potent anticancer agent **10c** in order to get insights about the possible underlying mechanism(s) for its antiproliferative activity. In addition, compound **10c** was evaluated for its kinase inhibitory effect against a panel of 21 oncogenic protein kinases and showed a significant selectivity towards BRAF^{V600E} and p38 α kinases among the tested kinases. Molecular docking study was conducted for the target compounds to illustrate the relation between the observed BRAF^{V600E} and p38 α kinases inhibitory activity and the molecular interaction of each derivative. In addition, molecular dynamic simulation study was carried out for compound **10c** to study its conformational stability in the two kinases, the potential energy was calculated during the stimulation process in a time interval of 0.5 ns for 600 ns.

2. Materials and Methods

2.1. Chemistry

The intermediate compounds as well as the target compounds were purified by flash column chromatography using silica gel 60 (0.040–0.063 mm, 230–400 mesh ASTM) and technical grade solvents. ¹H NMR and ¹³C NMR analyses were carried out on a Bruker Avance 400 spectrometer using tetramethylsilane (TMS) as an internal standard. Melting points were measured on a Walden Precision Apparatus Electrothermal 9300 apparatus and were uncorrected. LC-MS analysis was conducted using the following system: Waters 2998 photodiode array detector, Waters 3100 mass detector, Waters SFO system fluidics organizer, Waters 2545 binary gradient module, Waters reagent manager, Waters 2767 sample manager, SunfireTM C¹⁸ column (4.6 \times 50 mm, 5 μ m particle size); Solvent gradient = 95% A at 0 min, 1% A at 5 min; solvent A: 0.035% trifluoroacetic acid (TFA) in water; solvent B: 0.035% TFA in MeOH; flow rate = 3.0 mL/min.; the AUC was calculated using Waters MassLynx 4.1 software. The solvents and liquid reagents were transferred using hypodermic syringes. All the solvents and reagents were purchased from commercial companies and used as such.

2.1.1. Synthesis of methyl 3-methoxybenzoate (**2**)

A mixture of 3-methoxybenzoic acid (**1**, 5 g, 0.03 mol) and methanol (50 mL) were heated under reflux until compound **1** was dissolved in methanol then few drops of concentrated sulfuric acid was added to the mixture and refluxed for 8 h. The resulting mixture was cooled to room temperature, diluted with water and a saturated solution of NaHCO₃ was added to the mixture to neutralize the benzoic acid, extracted with ethyl acetate, dried over anhydrous Na₂SO₄ and evaporated under vacuum to get the ester derivative **2**.

Yield: 90%; m.p.: 110–111°C; ¹H NMR (400 MHz, CDCl₃) δ 7.61 (m, 1H), 7.54 (m, 1H), 7.31 (t, *J* = 8.0 Hz, 1H), 7.07 (m, 1H) [Ar-H], 3.89 (s, 1H, OCH₃), 3.81 (s, 1H, OCH₃); ¹³C NMR (100 MHz, CDCl₃) δ 166.9, 159.9, 131.4, 129.6, 122.2, 119.4, 114.2 [Ar-C], 55.3 (OCH₃), 52.0 (OCH₃).

2.1.2. Synthesis of 2-(2-bromopyridin-4-yl)-1-(3-methoxyphenyl)ethan-1-one (**3**)

To a solution of 2-bromo-4-picoline (0.5 mL, 5.6 mmol) in THF (20 mL) at -70°C, LiHMDS (11 mL, 1.0 M solution in THF, 10.8 mmol) was slowly added under N₂ to the reaction mixture maintaining the temperature at -70°C. After 30 minutes, a solution of compound **2** (1.0 g, 5.0 mmol) in THF (10 mL) was slowly added to the reaction mixture under N₂ at -70°C. The resulting mixture was stirred for 6 hours at room temperature. The mixture was quenched with saturated aqueous NH₄Cl (20 mL), and ethyl acetate (30 mL) was added. The organic layer was separated, and the aqueous layer was extracted with ethyl acetate (3–10 mL). The combined organic layer was washed with saline and dried over anhydrous Na₂SO₄, evaporated under vacuum to yield the title compound **3**, which were subjected to the next step without further purification.

2.1.3. Synthesis of 1-(2-bromopyridin-4-yl)-2-(3-methoxyphenyl)ethane-1,2-dione (**4**)

A solution of compound **3** (2.0 g, 6.8 mmol) in DMSO (10 mL) was heated to 55°C. Hydrobromic acid (2.5 mL, 20.4 mmol) was added dropwise to the reaction mixture. The reaction was stirred at 55°C for 2 hours. The reaction mixture was poured carefully to a saturated solution of sodium bicarbonate, extracted with ethyl acetate, dried and evaporated to get the required compound **4**.

Yield: 80%; m.p.: 115–116°C; ¹H NMR (400 MHz, CDCl₃) δ 8.63 (d, *J* = 5.2 Hz, 1H), 7.97 (s, 1H), 7.75 (d, *J* = 1.2 Hz, 1H), 7.74 (d, *J* = 1.2 Hz, 1H), 7.48 (m, 2H), 7.26 (m, 1H) [Ar-H], 3.90 (s, 3H, OCH₃); ¹³C NMR (100 MHz, CDCl₃) δ 191.7, 191.0, 160.3, 151.6, 143.5, 141.2, 133.3, 130.3, 127.2, 123.4, 122.7, 121.3, 113.1 [Ar-C], 55.6 (OCH₃).

2.1.4. Synthesis of 2-bromo-4-(4-(3-methoxyphenyl)-2-(4-nitrophenyl)-1H-imidazol-5-yl)pyridine (**5**)

To a solution of compound **4** (1.23 g, 4 mmol) and 4-nitrobenzaldehyde (0.61 g, 4 mmol) in acetic acid (10 mL), ammonium acetate (3.1 g, 40 mmol) was added. The reaction mixture was heated to 100°C for 4 hours. The reaction mixture was poured in ammonia solution with crushed ice. The resulted precipitate was filtered, washed with water three times, and dried under vacuum to get the titled compound **5**.

Yield: 85%; m.p.: 203–204°C; ¹H NMR (400 MHz, CDCl₃) δ 8.37 (m, 2H), 8.26 (m, 3H), 7.85 (d, *J* = 0.8 Hz, 1H), 7.56 (dd, *J* = 1.6, 5.6 Hz, 1H), 7.45 (t, *J* = 8.0 Hz, 1H), 7.11 (m, 3H) [Ar-H], 3.85 (s, 3H, OCH₃); ¹³C NMR (100 MHz, CDCl₃) δ 160.1, 149.5, 149.3, 141.5, 130.0, 129.8, 127.0, 125.0, 120.9, 120.5, 118.3, 114.5, 114.2, 113.9 [Ar-C], 54.5 (OCH₃).

2.1.5. Synthesis of 4-(5-(2-bromopyridin-4-yl)-4-(3-methoxyphenyl)-1H-imidazol-2-yl)aniline (**6**)

To a solution of compound **5** (3.2 g, 7.13 mmol) in ethyl acetate (50 mL), SnCl₂·2H₂O (8.04 g, 35.6 mmol) was added portion wise while stirring at 0°C. The reaction temperature was raised gradually to 80°C and the reaction mixture was heated for 4 hours. The reaction progression was monitored by TLC. After reaction completion, the reaction mixture was neutralized by saturated solution of NaHCO₃, extracted by ethyl acetate (20 mL \times 3), dried over anhydrous Na₂SO₄, and evaporated under vacuum to produce the titled compound **6**. The formed residue was subjected to the next step reaction without further purification.

2.1.6. General procedure for synthesis of compounds **7a–d** and **8a,b**

To a solution of compound **6** (0.3 mmol) in anhydrous THF (6 mL) and DIPEA (78 mg, 0.6 mmol) at 0°C, the corresponding acyl chlorides or sulfonyl chlorides (0.36 mmol) was added dropwise. The reaction mixture was stirred at room temperature for 12 h. After reaction completion, the solvent was evaporated, and the residue was partitioned between ethyl acetate and water. The organic layer was separated, and the aqueous layer was extracted with ethyl acetate (thrice, 10 mL each time). The combined organic layers were washed with brine two times

and the organic solvent was evaporated under reduced pressure. The residue was purified by column chromatography (hexane: ethyl acetate 2:1 (v/v)) to obtain compounds **7a-d** and **8a,b**.

2.1.6.1. N-(4-(5-(2-Bromopyridin-4-yl)-4-(3-methoxyphenyl)-1H-imidazol-2-yl)phenyl)acetamide (7a). Yield: 74%; m.p.: 139-141°C; ¹H NMR (400 MHz, CDCl₃) δ 10.12 (s, 1H), 8.27 (d, *J* = 4.0 Hz, 1H), 8.02 (d, *J* = 8.4 Hz, 2H), 7.78 (s, 1H), 7.71 (d, *J* = 8.8 Hz, 2H), 7.50 (d, *J* = 3.6 Hz, 1H), 7.44 (s, 1H), 7.13 (d, *J* = 8.8 Hz, 2H), 7.07 (s, 1H) [Ar-H], 3.81 (s, 3H, OCH₃), 3.35 (s, 3H, CH₃); ¹³C NMR (100 MHz, CDCl₃) δ 168.8 (CO), 159.9, 150.8, 142.3, 140.4, 126.6, 124.9, 119.4 [Ar-C], 55.7 (OCH₃), 24.5 (CH₃); LC/MS 464.9 (M⁺ + 2).

2.1.6.2. N-(4-(5-(2-Bromopyridin-4-yl)-4-(3-methoxyphenyl)-1H-imidazol-2-yl)phenyl)propionamide (7b). Yield: 75%; m.p.: 121-123°C; ¹H NMR (400 MHz, CDCl₃) δ 8.30 (s, 1H), 8.10 (d, *J* = 5.2 Hz, 1H), 7.94 (d, *J* = 8.4 Hz, 2H), 7.77 (s, 1H), 7.54 (d, *J* = 8.4 Hz, 2H), 7.34 (d, *J* = 5.2 Hz, 1H), 7.29 (t, *J* = 12.0 Hz, 2H), 6.99 (t, *J* = 6.8 Hz, 2H), 6.92 (d, *J* = 8.0 Hz, 1H) [Ar-H], 3.75 (s, 3H, OCH₃), 2.21 (q, *J* = 7.2 Hz, 2H, CH₂CH₃), 1.03 (t, *J* = 7.6 Hz, 3H, CH₂CH₃); ¹³C NMR (100 MHz, CDCl₃) δ 173.5 (CO), 159.7, 149.6, 147.2, 142.4, 138.6, 130.1, 126.7, 125.3, 123.1, 120.4, 114.6, 114.1, 55.4 [Ar-C], 30.7 (CH₂CH₃), 9.1 (CH₂CH₃); LC/MS 478.8 (M⁺ + 2).

2.1.6.3. N-(4-(5-(2-Bromopyridin-4-yl)-4-(3-methoxyphenyl)-1H-imidazol-2-yl)phenyl)isobutyramide (7c). Yield: 80%; m.p.: 140-142°C; ¹H NMR (400 MHz, CDCl₃) δ 8.49 (s, 1H), 8.04 (d, *J* = 5.2 Hz, 1H), 7.83 (d, *J* = 8.0 Hz, 2H), 7.72 (s, 1H), 7.48 (d, *J* = 8.4 Hz, 2H), 7.29 (d, *J* = 2.8 Hz, 1H), 7.21 (t, *J* = 8.0 Hz, 1H), 6.93 (d, *J* = 7.6 Hz, 2H), 6.86 (d, *J* = 8.4 Hz, 1H) [Ar-H], 3.69 (s, 3H, OCH₃), 2.51-2.40 (m, 1H, CH(CH₃)₂), 1.10 (d, *J* = 6.8 Hz, 6H, CH(CH₃)₂); ¹³C NMR (100 MHz, CDCl₃) δ 176.6 (CO), 149.5, 147.3, 142.3, 138.8, 131.7, 130.0, 125.4, 121.0, 120.5, 114.5, 114.0 [Ar-C], 55.3 (OCH₃), 36.3 (CH(CH₃)₂), 19.45 (CH(CH₃)₂), 18.97 (CH(CH₃)₂); LC/MS 492.9 (M⁺ + 2).

2.1.6.4. N-(4-(5-(2-Bromopyridin-4-yl)-4-(3-methoxyphenyl)-1H-imidazol-2-yl)phenyl)benzamide (7d). Yield: 75%; m.p.: 151-153°C; ¹H NMR (400 MHz, CDCl₃) δ 8.81 (s, 1H), 8.03-8.02 (m, 2H), 7.88 (d, *J* = 7.6 Hz, 2H), 7.67 (d, *J* = 8.0 Hz, 3H), 7.58 (d, *J* = 8.0 Hz, 2H), 7.42 (t, *J* = 6.4 Hz, 2H), 7.14 (t, *J* = 7.6 Hz, 1H), 6.91 (d, *J* = 7.2 Hz, 2H), 6.79 (d, *J* = 7.2 Hz, 1H) [Ar-H], 3.64 (s, 3H, OCH₃); ¹³C NMR (100 MHz, CDCl₃) δ 167.4 (CO), 160.2, 149.3, 147.6, 144.8, 141.5, 139.7, 134.7, 131.6, 129.8, 129.3, 128.2, 127.3, 126.3, 125.1, 120.9, 120.5, 114.3 [Ar-C], 54.5 (OCH₃); LC/MS 526.9 (M⁺ + 2).

2.1.6.5. N-(4-(5-(2-Bromopyridin-4-yl)-4-(3-methoxyphenyl)-1H-imidazol-2-yl)phenyl)methanesulfonamide (8a). Yield: 80%; m.p.: 150-152°C; ¹H NMR (400 MHz, CDCl₃) δ 12.97 (brs, 1H, NH), 8.26 (s, 1H), 8.05 (d, *J* = 8.4 Hz, 2H), 7.77 (s, 1H), 7.50 (s, 1H), 7.45 (s, 1H), 7.32 (d, *J* = 8.4 Hz, 2H), 7.13 (d, *J* = 7.6 Hz, 2H), 7.08 (s, 1H) [Ar-H], 3.81 (s, 3H, OCH₃), 3.07 (s, 3H, SO₂CH₃); ¹³C NMR (100 MHz, CDCl₃) δ 160.0 (CO), 150.8, 142.3, 139.6, 130.6, 127.1, 125.5, 119.8 [Ar-C], 55.7 (OCH₃); LC/MS 500.9 (M⁺ + 2).

2.1.6.6. N-(4-(5-(2-Bromopyridin-4-yl)-4-(3-methoxyphenyl)-1H-imidazol-2-yl)phenyl)benzenesulfonamide (8b). Yield: 73%; m.p.: 127-129°C; ¹H NMR (400 MHz, CDCl₃) δ 12.08 (d, *J* = 5.2 Hz, 1H), 11.78 (d, *J* = 8.8 Hz, 2H), 11.75-11.73 (d, *J* = 8.0 Hz, 3H), 11.48-11.45 (m, 1H), 11.38-11.36 (m, 3H), 11.28 (t, *J* = 8.0 Hz, 1H), 11.15 (d, *J* = 7.2 Hz, 2H), 10.99-10.96 (m, 2H), 10.91 (d, *J* = 8.4 Hz, 3H) [Ar-H], 7.74 (s, 3H, OCH₃); ¹³C NMR (100 MHz, CDCl₃) δ 163.8, 153.4, 145.9, 143.3, 136.8, 134.0, 132.9, 130.9, 130.8, 129.4, 125.0, 124.7, 124.6, 118.5, 118.0 [Ar-C], 59.1 (OCH₃); LC/MS 562.8 (M⁺ + 2).

2.1.7. General procedure for synthesis of compounds 9a-d

To a solution of compound **6** (0.3 mmol) and DIPEA (78 mg, 0.6 mmol) in anhydrous THF (6 mL), the appropriate chloroformate (0.36 mmol) was added drop wise under nitrogen at 0°C. The reaction mixture was stirred at room temperature for 12 h. After reaction completion, the solvent was evaporated, and the residue was partitioned between ethyl acetate and water. The organic layer was separated and the aqueous layer was extracted with ethyl acetate (thrice, 10 mL each time). The combined organic layers were washed with brine two times and the organic solvent was evaporated under reduced pressure. The residue was purified by column chromatography (hexane: ethyl acetate 2:1 v/v) to obtain compounds **9a-d**.

2.1.7.1. Methyl (4-(5-(2-bromopyridin-4-yl)-4-(3-methoxyphenyl)-1H-imidazol-2-yl)phenyl)carbamate (9a). Yield: 77%; m.p.: 134-136°C; ¹H NMR (400 MHz, CDCl₃) δ 8.11 (d, *J* = 5.2 Hz, 1H), 7.84 (d, *J* = 8.0 Hz, 2H), 7.77 (s, 1H), 7.42 (d, *J* = 8.0 Hz, 2H), 7.36 (d, *J* = 4.8 Hz, 1H), 7.28 (t, *J* = 8.8 Hz, 2H), 6.97 (d, *J* = 12.0 Hz, 2H), 6.91 (d, *J* = 8.0 Hz, 1H) [Ar-H], 3.74 (s, 3H, OCH₃), 3.70 (s, 3H, COOCH₃); ¹³C NMR (100 MHz, CDCl₃) δ 160.0 (CO), 154.1, 149.8, 142.5, 130.2, 126.9, 125.5, 120.9, 120.5, 118.8, 114.9, 114.0 [Ar-C], 60.5 (COOCH₃), 55.4 (OCH₃); LC/MS 480.8 (M⁺ + 2).

2.1.7.2. Ethyl (4-(5-(2-bromopyridin-4-yl)-4-(3-methoxyphenyl)-1H-imidazol-2-yl)phenyl)carbamate (9b). Yield: 76%; m.p.: 140-142°C; ¹H NMR (400 MHz, CDCl₃) δ 8.08 (d, *J* = 5.2 Hz, 1H), 7.83 (d, *J* = 8.4 Hz, 2H), 7.76 (s, 1H), 7.41 (d, *J* = 8.0 Hz, 2H), 7.34 (d, *J* = 4.8 Hz, 1H), 7.27 (t, *J* = 8.4 Hz, 1H), 7.21 (s, 1H), 6.98-6.96 (m, 2H), 6.91 (d, *J* = 8.0 Hz, 1H) [Ar-H], 4.12 (q, *J* = 6.4 Hz, 2H, CH₂CH₃), 3.73 (s, 3H, OCH₃), (t, *J* = 7.6 Hz, 3H, CH₂CH₃); ¹³C NMR (100 MHz, CDCl₃) δ 159.9 (CO), 153.8, 149.6, 147.1, 142.3, 139.1, 131.5, 130.1, 126.7, 125.9, 124.2, 120.9, 120.4, 118.5, 114.7, 113.9 [Ar-C], 61.5 (CH₂CH₃), 55.35 (OCH₃), 14.46 (CH₂CH₃); LC/MS 494.9 (M⁺ + 2).

2.1.7.3. Isopropyl (4-(5-(2-bromopyridin-4-yl)-4-(3-methoxyphenyl)-1H-imidazol-2-yl)phenyl)carbamate (9c). Yield: 82%; m.p.: 141-143°C; ¹H NMR (400 MHz, CDCl₃) δ 8.04 (d, *J* = 5.2 Hz, 1H), 7.82 (d, *J* = 8.4 Hz, 2H), 7.73 (s, 1H), 7.38 (d, *J* = 8.4 Hz, 2H), 7.31 (d, *J* = 4.8 Hz, 1H), 7.23 (t, *J* = 8.4 Hz, 2H), 6.92 (t, *J* = 2.0 Hz, 2H), 6.87 (d, *J* = 8.0 Hz, 1H), 4.95-4.89 (m, 1H, CH(CH₃)₂), 3.70 (s, 3H, OCH₃), 1.25 (d, *J* = 6.0 Hz, 6H, CH(CH₃)₂); ¹³C NMR (100 MHz, CDCl₃) δ 159.8 (CO), 153.4, 149.5, 142.3, 142.3, 139.1, 130.1, 126.2, 125.4, 124.2, 120.9, 119.8, 114.6, 113.3 [Ar-C], 69.2 (CH(CH₃)₂), 55.31 (OCH₃), 22.02 (CH(CH₃)₂); LC/MS 508.9 (M⁺ + 2).

2.1.7.4. Phenyl (4-(5-(2-bromopyridin-4-yl)-4-(3-methoxyphenyl)-1H-imidazol-2-yl)phenyl)carbamate (9d). Yield: 68%; m.p.: 184-186°C; ¹H NMR (400 MHz, CDCl₃) δ 8.13 (d, *J* = 5.2 Hz, 1H), 7.91 (d, *J* = 8.0 Hz, 2H), 7.77 (s, 1H), 7.53 (d, *J* = 7.6 Hz, 2H), 7.38 (d, *J* = 4.8 Hz, 1H), 7.29-7.26 (m, 4H), 7.19 (d, *J* = 7.6 Hz, 1H), 7.10 (d, *J* = 7.2 Hz, 2H), 6.97 (s, 2H), 6.91 (d, *J* = 8.4 Hz, 1H) [Ar-H], 3.73 (s, 3H, OCH₃); ¹³C NMR (100 MHz, CDCl₃) δ 160.0 (CO), 152.1, 150.9, 146.7, 143.2, 139.7, 132.8, 132.2, 131.8, 130.6, 129.8, 126.7, 124.9, 124.4, 122.7, 120.4, 118.9, 115.7, 114.8 [Ar-C], 55.7 (OCH₃); LC/MS 542.8 (M⁺ + 2).

2.1.8. General procedure for synthesis of compounds 10a-d, 11a,b, and 12a-d

To a solution of compound **7a-d**, **8a,b**, or **9a-d** (0.3 mmol) and tetrabutylammonium iodide (0.06 mmol, 0.2 eq.) in methylene chloride (3 mL), BBr₃ (3 mL of 1M solution in methylene chloride) was added drop wise at -78°C under N₂. The reaction mixture was stirred at the same temperature for 1 h, and then allowed to warm to room temperature and stirred for another 3 h. The mixture was quenched with saturated aqueous Na₂CO₃. Methylene chloride (5 mL) was added and the organic layer was separated. The aqueous layer was extracted with ethyl acetate

(5 mL x 2). The combined organic layer extracts were washed with brine and dried over anhydrous Na_2SO_4 . After evaporation of the organic solvent, the residue was purified by short column chromatography (methylene chloride: methanol 10:1 v/v) to yield the title compounds.

2.1.8.1. *N*-(4-(5-(2-Bromopyridin-4-yl)-4-(3-hydroxyphenyl)-1H-imidazol-2-yl)phenyl)acetamide (10a). Yield: 65%; m.p.: 192-194°C; ^1H NMR (400 MHz, CD_3OD) δ 8.19 (d, J = 5.2 Hz, 1H), 7.95 (d, J = 8.4 Hz, 2H), 7.81 (s, 1H), 7.72 (d, J = 8.8 Hz, 2H), 7.51 (s, 1H), 7.33 (t, J = 7.6 Hz, 1H), 6.99 (s, J = 7.6 Hz, 1H), 6.95 (s, 1H), 6.91 (d, J = 8.0 Hz, 1H) [Ar-H], 2.17 (s, 3H, COCH_3); ^{13}C NMR (100 MHz, CD_3OD) δ 170.4 (CO), 157.8, 149.3, 141.6, 129.9, 126.2, 125.1, 120.8, 119.7, 119.6, 115.4 [Ar-C], 22.5 (COCH_3); LC/MS 450.8 ($\text{M}^+ + 2$).

2.1.8.2. *N*-(4-(5-(2-Bromopyridin-4-yl)-4-(3-hydroxyphenyl)-1H-imidazol-2-yl)phenyl)propionamide (10b). Yield: 62%; m.p.: 162-164°C; ^1H NMR (400 MHz, CD_3OD) δ 8.13 (d, J = 5.6 Hz, 1H), 7.89 (d, J = 8.8 Hz, 2H), 7.76 (d, J = 6.8 Hz, 1H), 7.68 (d, J = 8.4 Hz, 2H), 7.46-7.45 (m, 1H), 7.34-7.31 (m, 1H), 6.95 (d, J = 7.2 Hz, 1H), 6.91-6.89 (m, 1H) [Ar-H], 2.41 (q, J = 7.6 Hz, 2H, COCH_2CH_3), 1.21 (t, J = 7.6 Hz, 3H, COCH_2CH_3); ^{13}C NMR (100 MHz, CD_3OD) δ 174.1 (CO), 160.3, 157.7, 149.3, 147.5, 144.9, 141.5, 139.7, 131.8, 129.9, 126.2, 125.1, 124.5, 120.9, 119.6, 115.6, 113.5 [Ar-C], 29.7 (COCH_2CH_3), 8.8 (COCH_2CH_3); LC/MS 464.8 ($\text{M}^+ + 2$).

2.1.8.3. *N*-(4-(5-(2-Bromopyridin-4-yl)-4-(3-hydroxyphenyl)-1H-imidazol-2-yl)phenyl)isobutyramide (10c). Yield: 65%; m.p.: 166-168°C; ^1H NMR (400 MHz, CD_3OD) δ 8.14 (d, J = 5.2 Hz, 1H), 7.92 (d, J = 8.8 Hz, 2H), 7.77 (s, 1H), 7.73 (d, J = 8.4 Hz, 2H), 7.48-7.46 (m, 1H), 7.30 (t, J = 8.0 Hz, 1H), 6.95-6.92 (m, 2H), 6.90-6.89 (m, 1H) [Ar-H], 2.75-2.65 (m, 1H, $\text{COCH}(\text{CH}_3)_2$), 1.22 (d, J = 6.8 Hz, 6H, $\text{COCH}(\text{CH}_3)_2$); ^{13}C NMR (100 MHz, CD_3OD) δ 177.4 (CO), 157.7, 149.3, 147.5, 144.8, 141.5, 139.9, 121.7, 130.7, 129.9, 126.3, 125.1, 124.6, 120.5, 119.8, 119.3, 115.7, 115.4 [Ar-C], 38.7 ($\text{COCH}(\text{CH}_3)_2$), 18.6 ($\text{COCH}(\text{CH}_3)_2$); LC/MS 478.9 ($\text{M}^+ + 2$).

2.1.8.4. *N*-(4-(5-(2-Bromopyridin-4-yl)-4-(3-hydroxyphenyl)-1H-imidazol-2-yl)phenyl)benzamide (10d). Yield: 60%; m.p.: 163-165°C; ^1H NMR (400 MHz, CD_3OD) δ 10.43 (brs, 1H), 8.27 (d, J = 4.8 Hz, 1H), 8.09 (d, J = 8.4 Hz, 2H), 7.99 (d, J = 5.6 Hz, 2H), 7.94 (d, J = 8.4 Hz, 2H), 7.78 (s, 1H), 7.65-7.63 (m, 1H), 7.57 (t, J = 7.6 Hz, 2H), 7.52 (d, J = 5.2 Hz, 1H), 7.32 (t, J = 7.6 Hz, 1H), 6.98-6.97 (m, 3H), 6.89 (d, J = 6.4 Hz, 2H); ^{13}C NMR (100 MHz, CD_3OD) δ 166.1 (CO), 158.2, 150.7, 142.3, 140.2, 135.3, 132.2, 128.9, 128.4, 126.4, 120.7 [Ar-C]; LC/MS 512.8 ($\text{M}^+ + 2$).

2.1.8.5. *N*-(4-(5-(2-Bromopyridin-4-yl)-4-(3-hydroxyphenyl)-1H-imidazol-2-yl)phenyl)methanesulfonamide (11a). Yield: 70%; m.p.: 148-150°C; ^1H NMR (400 MHz, CD_3OD) δ 8.17 (d, J = 5.2 Hz, 1H), 7.97 (d, J = 8.4 Hz, 2H), 7.80 (s, 1H), 7.50-7.49 (m, 1H), 7.38 (d, J = 8.8 Hz, 2H), 7.32 (t, J = 8.0 Hz, 1H), 6.99-6.90 (m, 3H) [Ar-H], 3.05 (s, 3H, SO_2CH_3); ^{13}C NMR (100 MHz, CD_3OD) δ 157.8, 149.3, 147.3, 144.9, 141.6, 139.3, 131.7, 129.9, 126.9, 125.1, 120.5, 119.9, 115.7, 115.4 [Ar-C], 38.2 (SO_2CH_3); LC/MS 486.7 ($\text{M}^+ + 2$).

2.1.8.6. *N*-(4-(5-(2-Bromopyridin-4-yl)-4-(3-hydroxyphenyl)-1H-imidazol-2-yl)phenyl)benzenesulfonamide (11b). Yield: 68%; m.p.: 152-154°C; ^1H NMR (400 MHz, CD_3OD) δ 8.10 (t, J = 5.2 Hz, 1H), 7.91-7.89 (m, 1H), 7.84 (t, J = 2.8 Hz, 1H), 7.82 (t, J = 2.0 Hz, 1H), 7.62 (d, J = 1.6 Hz, 1H), 7.52-7.51 (m, 2H), 7.49 (s, 1H), 7.45-7.44 (m, 2H), 7.29 (t, J = 0.8 Hz, 1H), 7.23-7.22 (m, 1H), 6.94 (d, J = 1.6 Hz, 1H), 6.92 (d, J = 1.2 Hz, 1H), 6.90-6.88 (m, 1H); ^{13}C NMR (100 MHz, CD_3OD) δ 157.7, 149.3, 147.2, 142.1, 141.6, 139.2, 136.1, 134.2, 132.7, 130.0, 128.3, 127.5, 126.8, 126.3, 126.1, 125.1, 120.5, 119.7, 115.8, 115.4; LC/MS 548.9 ($\text{M}^+ + 2$).

2.1.8.7. Methyl (4-(5-(2-bromopyridin-4-yl)-4-(3-hydroxyphenyl)-1H-imidazol-2-yl)phenyl)carbamate (12a). Yield: 72%; m.p.: 125-127°C; ^1H NMR (400 MHz, CD_3OD) δ 8.14 (d, J = 6.8 Hz, 1H), 7.88 (d, J = 8.8 Hz, 2H), 7.78 (s, 1H), 7.56 (d, J = 8.4 Hz, 2H), 7.48-7.47 (m, 1H), 7.31 (t, J = 7.6 Hz, 1H), 6.98-6.95 (m, 2H), 6.90-6.89 (m, 1H) [Ar-H], 3.76 (s, 3H, COOCH_3); ^{13}C NMR (100 MHz, CD_3OD) δ 157.8 (CO), 157.7, 154.6, 150.2, 149.3, 147.7, 145.0, 142.2, 140.1, 131.9, 130.1, 129.9, 127.0, 126.3, 125.0, 123.5, 120.5, 118.7, 115.4 [Ar-C], 51.27 (COOCH_3); LC/MS 466.8 ($\text{M}^+ + 2$).

2.1.8.8. Ethyl (4-(5-(2-bromopyridin-4-yl)-4-(3-hydroxyphenyl)-1H-imidazol-2-yl)phenyl)carbamate (12b). Yield: 70%; m.p.: 157-159°C; ^1H NMR (400 MHz, CD_3OD) δ 8.17 (d, J = 4.8 Hz, 1H), 7.90 (d, J = 8.4 Hz, 2H), 7.57 (d, J = 8.0 Hz, 2H), 7.49 (d, J = 4.4 Hz, 1H), 7.31 (t, J = 7.6 Hz, 1H), 6.96 (t, J = 3.6 Hz, 2H), 6.90 (d, J = 7.6 Hz, 1H), 4.21 (q, J = 6.4 Hz, 2H, $\text{COOCH}_2\text{CH}_3$), 1.33 (t, J = 6.8 Hz, 3H, $\text{COOCH}_2\text{CH}_3$); ^{13}C NMR (100 MHz, CD_3OD) δ 157.8 (CO), 154.5, 149.3, 147.8, 141.5, 140.2, 129.9, 126.3, 125.1, 123.7, 120.5, 119.7, 118.3, 115.6, 115.4 [Ar-C], 60.66 ($\text{COOCH}_2\text{CH}_3$), 13.52 ($\text{COOCH}_2\text{CH}_3$); LC/MS 480.8 ($\text{M}^+ + 2$).

2.1.8.9. Isopropyl (4-(5-(2-bromopyridin-4-yl)-4-(3-hydroxyphenyl)-1H-imidazol-2-yl)phenyl)carbamate (12c). Yield: 62%; m.p.: 177-179°C; ^1H NMR (400 MHz, CD_3OD) δ 8.17 (d, J = 5.2 Hz, 1H), 7.78 (d, J = 0.8 Hz, 1H), 7.75 (d, J = 2.4 Hz, 1H), 7.73-7.72 (m, 1H), 7.49-7.48 (m, 1H), 7.31 (t, J = 8.0 Hz, 1H), 6.94-6.93 (m, 1H), 6.90-6.87 (m, 3H), 6.81 (d, J = 2.4 Hz, 1H) [Ar-H], 4.89 (m, 1H, $\text{CH}(\text{CH}_3)_2$), 4.13-4.09 (d, J = 6.8 Hz, 6H, $\text{CH}(\text{CH}_3)_2$); ^{13}C NMR (100 MHz, CD_3OD) δ 157.7 (CO), 149.5, 149.3, 149.9, 141.5, 129.8, 127.9, 127.0, 120.4, 119.7, 118.3, 115.5, 115.3, 114.6 [Ar-C], 19.5 ($\text{CH}(\text{CH}_3)_2$), 13.1 ($\text{CH}(\text{CH}_3)_2$); LC/MS 494.7 ($\text{M}^+ + 2$).

2.1.8.10. Phenyl (4-(5-(2-bromopyridin-4-yl)-4-(3-hydroxyphenyl)-1H-imidazol-2-yl)phenyl)carbamate (12d). Yield: 64%; m.p.: 174-176°C; ^1H NMR (400 MHz, CD_3OD) δ 8.14 (d, J = 5.2 Hz, 1H), 7.94 (t, J = 7.6 Hz, 2H), 7.79 (s, 1H), 7.64 (t, J = 8.0 Hz, 2H), 7.48 (d, J = 5.2 Hz, 1H), 7.41 (t, J = 7.6 Hz, 3H), 7.33-7.29 (m, 2H), 7.20 (d, J = 7.6 Hz, 3H), 6.98 (s, 1H), 6.96 (d, J = 2.4 Hz, 1H), 6.91 (d, J = 6.4 Hz, 1H); ^{13}C NMR (100 MHz, CD_3OD) δ 158.3 (CO), 157.7, 152.6, 150.8, 149.3, 141.7, 140.2, 139.7, 133.9, 129.9, 129.1, 126.4, 125.3, 124.3, 121.5, 120.5, 119.7, 118.5, 115.6, 115.4 [Ar-C]; LC/MS 528.8 ($\text{M}^+ + 2$).

2.2. Biological assays

2.2.1. Anticancer screening

The anticancer screening of the final target compounds (**7a-d**, **8a,b**, **9a-d**, **10a-d**, **11a,b**, and **12a-d**) against a panel of 60 human cancer cell lines was carried out using the sulforhodamine B (SRB) assay at the NCI, Bethesda, Maryland, USA adopting the standard protocol (https://dtp.cancer.gov/discovery_development/nci-60/methodology.htm). The details of the screening protocol are included in the Supplementary File.

2.2.2. Cell-based mechanistic assays

2.2.2.1. Cell cultures and treatment. K562 (human leukemia), MCF-7 (human breast cancer) and HT-29 (human colon cancer) cells were maintained in RPMI complete medium supplemented with 10% fetal bovine serum (FBS), penicillin (100 units/mL) and streptomycin (100 $\mu\text{g/mL}$). The cells were incubated in a humidified incubator at 37°C with 5% CO_2 . The cells were seeded in the cell culture dishes and treated with compound **10c** at different doses (half, equal, and double of the respective IC_{50} values) for 24 h.

2.2.2.2. Flow cytometry analysis of cell cycle induced by compound 10c. The cell cycle was analyzed on K562, MCF-7 and HT-29 cells by treating

with compound **10c** with different doses for 24 h. Cells were then harvested, fixed on ice with 70% of ethyl alcohol, followed by centrifugation, washing and resuspended in PBS (250 μ L). RNA was degraded by treating with 100 μ g/mL RNase A (100 μ L) for 30 min at 37°C. DNA was stained with 200 μ L from 50 μ g/mL propidium iodide (Thermo Fisher; P3566) for 30 min at 37°C in dark condition. The cell cycle was analyzed by flow cytometry using BD FACSCanto II flow cytometer (BD Biosciences). The obtained data were analyzed using FlowJo analysis software version 10.7.2.

2.2.2.3. Apoptosis analysis by annexin V and propidium iodide staining. Cells were plated in 6-well plates and allowed to grow until ~70% of confluency. The cells were then treated with compound **10c** with different doses for 24 h. After the incubation period, the cells were harvested, centrifuged, and resuspended in 200 μ L annexin binding buffer (10 mM HEPES, 140 mM NaCl, 2.5 mM CaCl_2 ; pH 7.4). After that, 5 μ L of annexin V Alexa Fluor™ 488 (Thermo Fisher; A13201) and 200 μ L propidium iodide from 50 μ g/mL stock (Thermo Fisher; P3566) was added for 30 min on ice in dark condition. An additional 300 μ L annexin binding buffer was added, the suspension was mixed gently, and apoptosis was analyzed by flow cytometry using BD FACSCanto II flow cytometer (BD Biosciences). The obtained data were analyzed using FlowJo analysis software version 10.7.2.

2.2.2.4. Western blot analysis. Compound-treated cells were harvested, washed twice with ice-cold PBS, lysed in lysis buffer containing 50 mM HEPES (pH 7.5), 150 mM NaCl, 1.5 mM MgCl_2 , 5 mM KCl, 0.1% Tween-20, 2 mM DTT, and protease inhibitor cocktail (Roche), incubated on ice for 10 min and centrifuged at $15,000 \times g$ for 10 min. Supernatants were collected as whole cell lysates and a quantity of 20 μ g of total protein was loaded in each well, separated by 12% sodium dodecyl sulfate polyacrylamide gel electrophoresis (SDS-PAGE) and transferred onto nitrocellulose membranes (Millipore, MA, USA). The membranes were blocked with 5% skimmed milk for 2 h at room temperature and then incubated with the following primary antibodies overnight at 4°C: anti-Bcl-1 monoclonal antibody (1:1000 dilution, Santacruz, sc-48341) and anti- β -actin polyclonal antibody (1:2500, AbFrontier, LF-PA0207). After being washed with TBST buffer (Tris-buffered saline supplemented with Tween-20) thrice for 10 min, the membranes were incubated with corresponding horseradish peroxidase-conjugated secondary antibody for 1 hr at room temperature. After another three washes with TBST, the proteins band bound with the antibodies were visualized with an enhanced electro chemiluminescence (ECL) system.

2.2.3. *In vitro* BRAF^{V600E}/p38 α kinase inhibition assay

Reaction Biology Corp. Kinase HotSpotSM service was used for screening of final compounds (Anastassiadis et al., 2011). Assay protocol was applied using 1 μ M concentration of ATP as following:

2.2.3.1. Reagents. Base reaction buffer: 20 mM Hepes (pH 7.5), 10 mM MgCl_2 , 1 mM EGTA, 0.01% Brij35, 0.02 mg/ml BSA, 0.1 mM Na_3VO_4 , 2 mM DTT, 1% DMSO.

Required cofactors are added individually to each kinase reaction.

2.2.3.2. Procedure.

- 1 Prepare substrate in freshly prepared base reaction buffer.
- 2 Deliver any required cofactors to the substrate solution above.
- 3 Deliver indicated kinase into the substrate solution and gently mix.
- 4 Deliver compounds in 100% DMSO into the kinase reaction mixture by Acoustic technology (Echo550; nanoliter range), incubate for 20 minutes at room temperature.

5 Deliver ^{33}P -ATP into the reaction mixture to initiate the reaction.

6 Incubate kinase reaction for 2 hours at room temperature.

7 Detect kinase activity by P81 filter-binding method.

2.3. Docking study

The X-ray crystal structures of BRAF^{V600E} oncogenic mutant kinase in complex with GDC0879 (PDB ID: 4MNF) and p38 α kinase in complex with TAK-715 (PDB ID: 3ZSG) were downloaded from the protein data bank (www.rcsb.org) in PDB format. The 2D structure of the target compounds were drawn using ChemDraw software. Molecular Operating Environment (MOE, 2014.0901) software was used for the molecular docking operation of the target compounds **7a-d**, **8a,b**, **9a-d**, **10a-d**, **11a,b**, and **12a-d** with BRAF^{V600E} kinase enzyme domain (PDB ID: 4MNF) and p38 α kinase enzyme domain (PDB ID: 3ZSG). Both kinases were prepared for the molecular docking procedure by applying 3D protonation of both enzyme amino acids and the native ligands (GDC0879 and TAK-715). In addition, water of crystallization was removed from both BRAF^{V600E} kinase and p38 α kinase domains. The active site of both enzymes was isolated. The docking simulation of native ligands (GDC0879 and TAK-715) with the active site of BRAF^{V600E} kinase and p38 α kinase was investigated in order to validate the docking protocol. Both 3D protonation and energy minimization were performed for the target compounds using MOE, 2014.0901 software.

2.4. Molecular dynamic simulation

The molecular dynamic (MD) simulation study was carried out for the obtained docked protein complex of the native ligands GDC0879 and TAK-715 with compound **10c**, using standard default parameter setting in the MOE 2014 software in order to examine the conformational stability of their docked complexes in the active site of the corresponding kinase BRAF^{V600E} (PDB ID: 4MNF) and p38 α kinase (PDB ID: 3ZSG).

MOE implemented four algorithms, the Nos_e-Poincar_e-Andersen (NPA), the Nos_e-Hoover-Andersen (NHA), Berendsen velocity/position (BER) and Nanoscale Molecular Dynamics (NAMD). In this study, MD calculations were performed by using NPA, the most precise algorithm for long-time simulations.⁵¹ The system optimization was obtained by energy minimization, applying MMFF94x force field, water as a solvent, six margins and delete far existing solvent with distance greater than 4 Å. The MD simulation protocol was run for 600 ns at 300 K temperature; the potential energy (kcal/mole) was recorded at intervals of 0.5 ns. Also, the root mean square deviation (RMSD) values were observed during the whole MD simulation process in order to determine the stability of the ligand-receptor complex during the MD simulation.

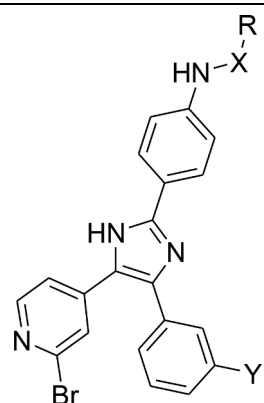
3. Results and discussion

3.1. Chemistry

The designed compounds **7a-d**, **8a,b**, **9a-d**, **10a-d**, **11a,b**, and **12a-d** were synthesized according to the reactions adopted in Scheme 1. 3-Methoxy-4-chlorobenzoic acid (**1**) was esterified using methanol and sulfuric acid to produce methyl ester analogue **2**. In presence of lithium bis(trimethylsilyl)amide (LiHMDS), the methyl group of 2-bromo-4-methylpyridine was activated by stirring for half an hour, followed by dropwise addition of the methyl ester **2** produced the 2-(2-bromopyridin-4-yl)-1-(3-methoxyphenyl)ethan-1-one intermediate **3**. Cyclization to the corresponding imidazole intermediate **5** was carried out by oxidation of **3** by HBr/DMSO to produce compound **4**, and subsequent

Table 1

Structures of the final target compounds **7a-d**, **8a,b**, **9a-d**, **10a-d**, **11a,b**, and **12a-d**.



Comp. No.	R	X	Y	Comp. No.	R	X	Y
7a	CH ₃	CO	OCH ₃	10a	CH ₃	CO	OH
7b	CH ₂ CH ₃	CO	OCH ₃	10b	CH ₂ CH ₃	CO	OH
7c	CH	CO	OCH ₃	10c	CH	CO	OH
	(CH ₃) ₂				(CH ₃) ₂		
7d	Ph	CO	OCH ₃	10d	Ph	CO	OH
8a	CH ₃	SO ₂	OCH ₃	11a	CH ₃	SO ₂	OH
8b	Ph	SO ₂	OCH ₃	11b	Ph	SO ₂	OH
9a	CH ₃	COO	OCH ₃	12a	CH ₃	COO	OH
9b	CH ₂ CH ₃	COO	OCH ₃	12b	CH ₂ CH ₃	COO	OH
9c	CH	COO	OCH ₃	12c	CH	COO	OH
	(CH ₃) ₂				(CH ₃) ₂		
9d	Ph	COO	OCH ₃	12d	Ph	COO	OH

reaction of **4** with 4-nitrobenzaldehyde in presence of ammonium acetate and acetic acid afforded compound **5**. The key nitro intermediate **5** was reduced to the corresponding amine derivative **6** by SnCl₂·2H₂O in ethyl acetate.

The final target compounds **7a-d** and **8a,b** were obtained by coupling of compound **6** with different acyl chlorides or sulfonyl chlorides in THF using DIPEA at room temperature. However, the carbamate derivatives **9a-d** were obtained by coupling of compound **6** with different chloroformates in THF under nitrogen at 0 °C. Demethylation was implemented by slow addition of boron tribromide at -70 °C under inert atmosphere in presence of catalytic amount of tetrabutylammonium iodide in dry methylene chloride to get the hydroxyl analogues **10a-d**, **11a,b** and **12a-d**. The target compounds structures are shown in Table 1.

3.2. Biological Screening

3.2.1. In vitro screening of the anticancer activity

3.2.1.1. Single dose testing against NCI-60 cell line panel. The methoxy-possessing derivatives were first synthesized with a degree of structural variation. Compounds **7a-d** (amides), **8a,b** (sulfonamides), and **9a-d** (carbamates) were submitted to National Cancer Institute (NCI) for evaluation of their antiproliferative activity over a panel of 60 human cancer cell lines representing nine human cancer types including leukemia, non-small cell lung (NSCL), colon, central nervous system (CNS), melanoma, ovarian, renal, prostate, and breast cancer cell lines. The compounds were pre-screened in a single dose concentration of 10 μM. The mean percentages of growth inhibition (% GI) of the tested compounds are depicted in Table 2, Table S1. The compounds molar refractivity (MR) and LogP values were calculated by ChemDraw software, in attempt to correlate the molecular properties for each compound and its observed activity Table 2.

Generally, the preliminary % GI results revealed that amide substituted derivatives **7a-d** showed the highest activity, followed by the

Table 2

Mean % growth inhibition (GI) values of compounds **7a-d**, **8a,b**, **9a-d**, **10a-d**, **11a,b**, and **12a-d** over the NCI 60 cell line panel at 10 μM concentration.

Cpd. ID	Mean % GI ^a	MR (cm ³ /mol)	LogP
7a	27.34	121.09	3.9
7b	44.61	125.83	4.55
7c	72.15	130.75	5.12
7d	81.83	141.22	5.8
8a	32.95	126.51	3.21
8b	75.42	144.99	5.4
9a	48.41	123.05	4.48
9b	70.59	127.85	4.82
9c	79.59	132.54	5.14
9d	2.56	142.13	6.15
10a	26.49	115.65	3.63
10b	40.39	120.4	4.29
10c	59.39	125.32	4.86
10d	87.90	135.78	5.53
11a	24.94	121.08	2.95
11b	75.70	139.55	5.13
12a	48.96	117.61	4.22
12b	71.31	122.41	4.56
12c	37.80	127.1	4.88
12d	6.57	136.69	5.88

^a Mean % inhibition values are the averages of duplicate assays.

^bLogP and MR values were calculated by ChemDraw Professional 16.0.1 software.

carbamate substituted derivatives **9a-d**, then the sulfonamide substituted derivatives **8a,b**. It is also noticed that the bulkier the substituent on CO, SO₂, and COO, the higher % GI, except for the phenyl carbamate derivative **9d**, which showed a dramatic drop in activity. For example, phenyl substitution on amide (**7a**) and sulfonamide (**8b**) elevated the activity by three folds compared to the methyl substituted compounds **7a** and **8a**, the isopropyl substitution on both amide (**7c**) and carbamate (**9c**) improved the antiproliferative activity comparable to the methyl and ethyl substituted derivatives **7a**, **7b**, **9a**, and **9b**. On the other hand, the molecular descriptors, molar refractivity (MR) and partition coefficient (LogP) are key parameters in determining the molecule's activity. As revealed in Table 2, the methyl substituted compounds **7a**, **8a**, and **9a**, with the lowest MR (121.09, 126.51, and 123.05, respectively) and LogP (3.9, 3.21, and 4.4, respectively) values exhibited the lowest activity amongst the tested amide, sulfonamide, and carbamate derivatives, respectively. Elevation of MR and LogP values in ethyl, isopropyl, and phenyl exhibiting derivatives resulted in improving the anticancer activity. Whereas, compound **9d** with the highest LogP value of 6.15 demonstrated a dramatic reduction in the activity, which could be explained in two hypotheses, the first, drug lipophilicity shouldn't exceed certain limit to ensure drug's solubility in the aqueous phase surrounding the targeted cells, the second, substitution with phenyl group on carbamate, which itself has extra space (oxygen atom) compared to the amides and sulfonamides, could result in emigration of the phenyl carbamate moiety out of the employed enzymes pockets, that in turn, reduce the drug affinity, as well as the activity.

Further optimization was conducted, the methoxy derivatives were demethylated to their corresponding hydroxyl derivatives **10a-d**, **11a,b**, and **12a-d**, the compounds were evaluated for their anticancer activity. As demonstrated in Table 2, no significant changes are observed in the activity of the resulted hydroxyl derivatives from their methoxy precursors. Even though, demethylation of the isopropyl derivatives **7c** and **9c** to **10c** and **12c** reduced the anticancer activity by 12% and 40%, respectively. Interestingly, the activity order of the hydroxyl derivatives went in similar accordance of the methoxy derivatives, where the compounds of higher MR and LogP exhibited the higher activity, except for compound **12d** (the phenyl carbamate derivative). Among the employed cell lines panels, leukemia, CNS cancers, renal cancers, and breast cancers are the most sensitive cell lines after treatment with the

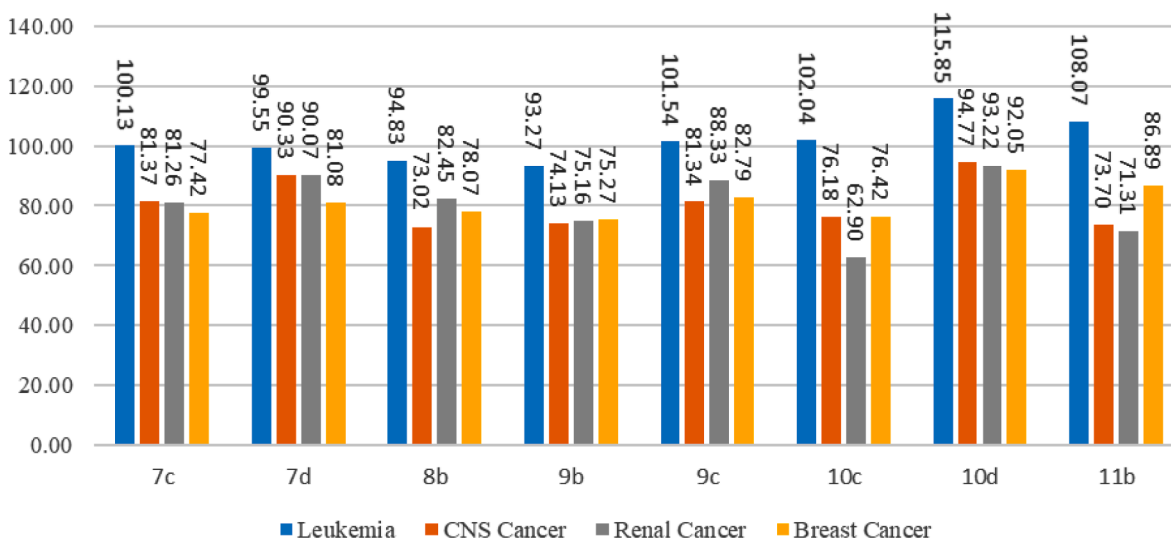


Fig. 2. Mean % GI of the most sensitive cancer types (leukemia, CNS cancers, renal cancers, and breast cancers) upon the treatment with compounds **7c**, **7d**, **8b**, **9b**, **9c**, **10c**, **10d**, and **11b** at 10 μ M concentration.

tested compounds. Compounds **7c**, **7d**, **8b**, **9b**, **9c**, **10c**, **10d**, and **11b** emerge to be the most potent antiproliferative agents among their synthesized subclasses and their mean % GI over the sensitive cell lines is illustrated in Fig. 2.

3.2.1.2. Five-dose testing against NCI-60 cell line panel. The most promising compounds **7c**, **7d**, **8b**, **9b**, **9c**, **10c**, **10d**, and **11b** were selected according to NCI criteria for further evaluation. The compounds were tested in a five-dose mode over the 60-cell lines panel in order to calculate their GI_{50} (the molar concentration causing 50% GI). Their potencies were compared with that of sorafenib, a multikinase anticancer drug, as a reference standard. As illustrated in Table 3, All the tested compounds showed high potency over all tested cell lines with sub-micromolar or one-digit micromolar GI_{50} values. Obviously, leukemia are the most sensitive cell lines, which are inhibited by all compounds at less than 3 μ M concentration. Moreover, the amide and carbamate grafting derivatives **7c**, **7d**, **9b**, **9c**, **10c**, and **10d** inhibited the growth of leukemia cell line RPMI-8226 at sub-micromolar concentrations below 600 μ M. Potent activity was observed against HCT-15 colon cancer cell line, which showed growth inhibition of $GI_{50} = 0.78$ and 0.33 μ M by compounds **7d** and **10c**, respectively. Among the employed CNS cancer cell lines, both SF-295 and SNB-75 demonstrated the highest sensitivity upon the treatment with compounds **7c**, **7d**, **9c**, **10c**, and **10d** which showed GI_{50} of 0.27–0.49 μ M, 0.23–0.81 μ M, 0.25–0.56 μ M, 0.20–0.17 μ M, and 0.34–0.28 μ M against the two cell lines, respectively. RXF 393 renal cancer cell line was highly inhibited by compounds **7c**, **7d**, **9b**, **9c**, **10c**, **10d** with GI_{50} values of 0.35, 0.26, 0.71, 0.28, 0.19, and 0.29 μ M, respectively. Most of the tested compounds exhibited high potency against HS 578T breast cancer cell line, which was inhibited at GI_{50} of 0.55, 0.34, 0.31, 0.22, and 0.31 μ M by compounds **7c**, **7d**, **9c**, **10c**, and **10d**, respectively. On the other hand, the rest of the evaluated cell lines showed moderate inhibition upon the treatment with the tested compounds. Apparently, compound **10c** emerged a broad-spectrum anticancer activity, and exhibited sub-micromolar activity over the tested cell lines (Fig. 3). In addition, compound **10c** showed incredible activity against MDA-MB-435 melanoma cell line with GI_{50} value of 70 nM. In comparison with the reference standard anticancer drug, sorafenib, compound **10c** exhibited superior potency than it against almost all the NCI-60 cell lines.

3.2.2. In vitro cell-based mechanistic assays

Due to the promising antiproliferative results of compound **10c**, further cell-based mechanistic studies were conducted including cell

cycle analysis, apoptosis induction, and autophagy analysis.

3.2.2.1. Cell cycle effects. To get certain insights about the underlying mechanism(s) of anticancer activity triggered by compound **10c**, its effects on cell cycle dynamics on K562, MCF-7, and HT29 cancer cell lines was evaluated. Cells were treated with **10c** with three different doses (half, equal, and double of the IC_{50} values) for 24 h. After that, cell cycle distribution was analyzed by flow cytometry (Fig. 4 & Tables 4, 5, and 6). As shown in Fig. 4, quantitative data after treatment with compound **10c** demonstrate that cell cycle was arrested in G2/M phase in K562 cells, G0/G1 phase in MCF-7 cells, and S phase in HT29 cells in a dose-dependent fashion compared with control. For example, the population of K562 cells at G2/M phase was increased from 27.60% (control) to 29.20% (148 nM) and 32.95% (296 nM) after treatment with compound **10c**. Similarly, increasing doses of compound **10c** was associated with remarkable accumulation of cells at G0/G1 phase in MCF-7 cells, as well as S phase in HT29 cells. Such cell cycle analysis strongly suggests the ability of compound **10c** to induce cell cycle perturbations in cancer cells.

3.2.2.2. Apoptosis induction in cancer cells. To further confirm the pro-apoptotic activity of compound **10c** in different cancer cells, the Annexin V and PI staining were performed. Flow cytometry analysis of the dual stained cells can distinguish cells into four stages, namely viable (Q4: Annexin V-negative/PI-negative), early apoptosis (Q3: Annexin V-positive/PI-negative), late apoptosis (Q2: Annexin V-positive/PI-positive) and necrotic cells (Q1: Annexin V-negative/PI-positive). Referring to the analyzed data (Fig. 5 & Tables 7, 8, and 9), compound **10c** demonstrate that total, early, and late apoptosis was increased in a dose-dependent manner compared with control in K562 cells significantly. For example, while the population of early apoptotic cells was 1.1% in control, their populations were 23.1% and 50.1% after treatment with 148 nM and 296 nM of compound **10c**. Early apoptotic cell percentages were significantly increased in the highest dose in HT29 cells whereas no significant apoptosis was happened in MCF-7 cells.

3.2.2.3. Autophagy analysis. The highly promising antiproliferative potency of compound **10c** encouraged us to conduct further mechanistic studies such as autophagy analysis. K562, MCF-7, and HT29 cell lines were exploited in this assay based on their availability in our labs and the high potency of compound **10c** against all of them ($IC_{50} = 0.15$, 0.10, and 0.37 μ M, respectively, Table 3).

Table 3

GI₅₀ values (μM) of 7c, 7d, 8b, 9b, 9c, 10c, 10d, 11b, and sorafenib over NCI-60 cell line panel.

Cell Lines	7c	7d	8b	9b	9c	10c	10d	11b	Sorafenib
Leukemia									
CCRF-CEM	2.99	3.15	3.14	2.76	2.22	0.31	1.32	1.91	2.00
HL-60(TB)	1.56	1.72	2.86	2.34	1.38	0.27	1.37	2.44	1.58
K-562	3.07	1.67	2.60	2.76	1.88	0.15	2.12	2.27	3.16
MOLT-4	2.56	2.70	2.74	2.21	1.64	0.38	2.00	2.01	3.16
RPMI-8226	0.51	0.39	2.49	0.79	0.39	0.31	0.59	2.35	1.58
SR	2.41	1.94	2.85	2.88	1.50	0.20	1.26	2.29	3.16
NSCLC									
A549/ATCC	3.45	4.07	3.11	3.07	2.96	0.43	2.95	3.00	3.16
EKVX	2.43	2.18	2.25	2.45	2.45	0.61	2.14	2.55	2.51
HOP-62	3.44	2.82	3.39	2.80	2.92	0.58	2.54	2.43	2.00
HOP-92	3.58	6.26	2.46	2.36	3.19	2.43	1.84	1.69	1.58
NCI-H226	2.53	2.95	2.91	2.21	2.46	0.79	2.33	2.25	2.00
NCI-H23	2.88	2.82	3.06	2.00	2.61	0.39	2.04	2.18	2.00
NCI-H322M	2.72	3.97	3.22	2.46	2.89	0.69	2.05	2.90	2.51
NCI-H460	3.20	3.53	2.85	2.79	2.99	0.33	2.45	2.14	2.51
NCI-H522	2.80	3.17	2.93	2.73	2.48	0.29	2.01	2.48	2.00
Colon Cancer									
COLO 205	2.81	3.55	2.66	3.23	3.26	0.40	1.99	2.42	2.00
HCC-2998	2.03	1.83	2.12	2.25	2.71	0.60	2.27	1.90	3.16
HCT-116	2.49	3.29	2.09	2.89	2.68	0.36	2.26	2.43	1.58
HCT-15	1.37	0.78	1.94	1.68	1.19	0.33	2.01	1.97	2.51
HT29	3.07	2.69	3.02	3.45	2.37	0.37	2.85	3.17	2.00
KM12	2.96	2.29	2.65	2.51	2.41	0.34	2.44	2.32	1.58
SW-620	3.52	3.77	2.83	3.19	3.32	0.37	2.37	2.84	2.51
CNS Cancer									
SF-268	4.07	6.13	3.33	3.26	3.35	1.41	2.21	3.18	2.51
SF-295	0.27	0.23	1.85	0.42	0.25	0.20	0.34	1.90	1.58
SF-539	1.78	1.59	2.53	1.76	1.53	0.31	1.51	2.01	1.58
SNB-19	3.76	3.87	4.03	2.96	3.19	0.44	1.83	3.32	3.16
SNB-75	0.49	0.81	1.92	2.14	0.56	0.17	0.28	1.30	3.16
U251	2.08	2.10	2.73	2.44	1.69	0.40	1.39	2.71	2.00
Melanoma									
LOX IMVI	1.61	1.13	1.56	1.56	1.49	0.56	1.52	1.74	1.58
MALME-3M	2.65	2.86	1.76	1.98	2.23	0.67	1.83	2.10	2.00
M14	3.30	2.91	2.03	2.40	3.06	0.31	1.82	2.50	2.00
MDA-MB-435	3.12	4.72	2.51	2.73	3.11	0.07	1.76	2.20	1.58
SK-MEL-2	2.30	2.93	2.50	2.58	2.33	0.54	2.02	2.41	2.00
SK-MEL-28	2.78	3.00	2.91	2.80	2.55	0.81	1.76	2.86	2.51
SK-MEL-5	1.80	1.79	1.87	1.83	1.88	0.51	1.79	2.40	1.58
UACC-257	4.02	5.34	3.11	2.68	3.15	2.20	2.21	2.53	2.00
UACC-62	2.57	2.95	2.58	1.89	1.98	0.25	1.73	1.91	1.58
Ovarian Cancer									
IGROV1	3.55	6.96	3.84	2.69	3.54	0.47	2.62	2.88	2.51
OVCAR-3	3.38	4.48	3.03	2.82	2.83	0.27	2.09	2.08	3.16
OVCAR-4	3.54	4.90	3.84	3.14	3.09	1.35	2.27	3.09	3.16
OVCAR-5	4.70	6.09	4.17	3.56	4.43	0.53	2.92	4.34	3.16
OVCAR-8	3.61	4.02	3.33	2.98	3.12	0.46	2.60	2.84	3.16
NCI/ADR-RES	3.03	3.55	3.44	2.35	2.85	ND	3.00	3.04	2.51
SK-OV-3	3.65	3.05	3.04	3.90	3.85	1.06	2.68	2.76	2.51
Renal Cancer									
786-0	1.30	0.70	2.98	2.16	0.97	0.38	1.08	2.51	3.16
A498	1.84	1.74	1.25	1.94	1.20	0.18	1.66	0.36	2.51
ACHN	2.74	2.95	2.60	2.62	2.70	0.77	2.43	2.55	2.51
CAKI-1	2.73	2.21	1.75	2.43	2.49	0.25	1.98	2.15	3.16
RXF 393	0.35	0.26	2.18	0.71	0.28	0.19	0.29	1.93	3.16
SN12C	3.31	ND	3.03	2.76	2.94	0.50	2.68	2.91	2.51
TK-10	4.35	6.92	3.72	3.88	3.61	2.05	2.92	3.04	3.98
UO-31	3.20	2.93	2.29	2.19	2.51	0.58	2.56	1.77	2.51
Prostate Cancer									
PC-3	3.01	3.25	2.39	2.52	2.62	0.35	1.90	2.12	2.00
DU-145	3.86	ND	3.69	3.24	3.33	0.42	2.76	3.24	3.16
Breast Cancer									
MCF7	1.67	2.40	2.64	2.13	1.59	0.10	1.29	2.30	2.51
MDA-MB-231/ATCC	4.09	3.97	3.23	3.27	3.85	0.53	2.59	2.71	1.26
HS 578T	0.55	0.34	1.71	1.68	0.31	0.22	0.31	1.50	2.51
BT-549	2.04	3.30	2.72	2.19	2.19	0.77	1.80	2.49	3.16
T-47D	2.65	2.44	2.74	1.96	2.08	0.55	1.73	2.44	1.58
MDA-MB-468	1.89	2.87	1.98	1.67	2.03	0.22	1.91	1.85	2.00

Bold figures indicate sub-micromolar IC₅₀ values and stronger potency than sorafenib.

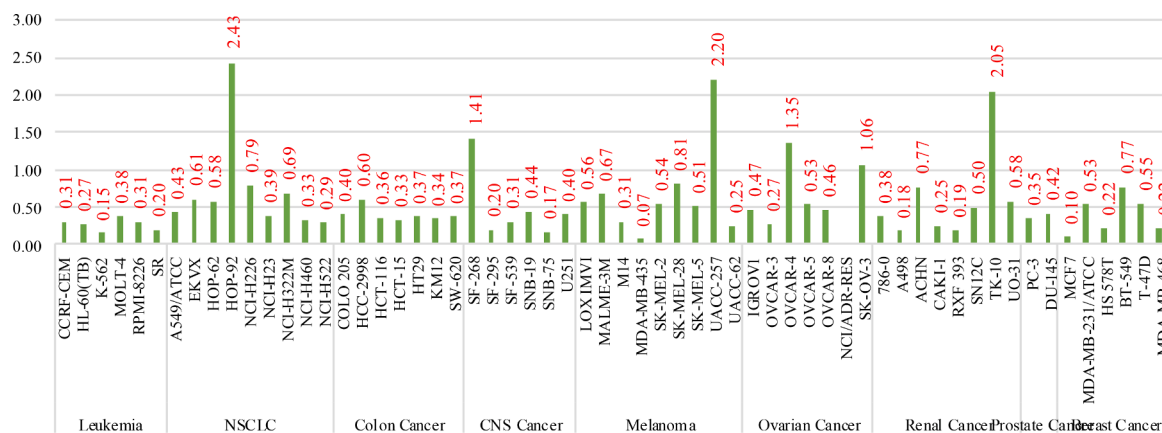


Fig. 3. GI₅₀ values of compound 10c against the employed 60 human cancer cell lines panel.

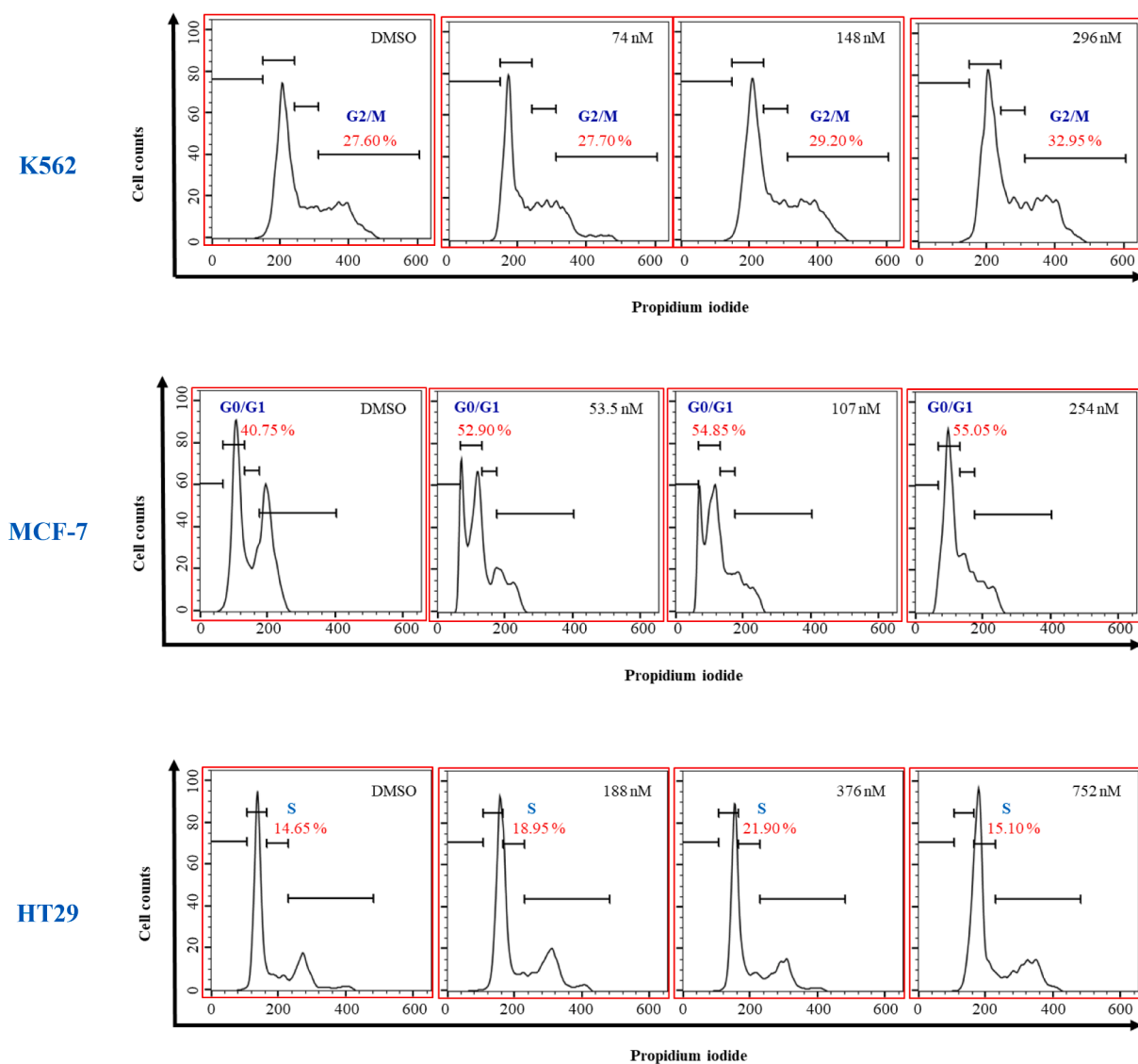


Fig. 4. Flow cytometric analysis of compound 10c on cell cycle phase distribution in different cells using propidium iodide stains detected by flow cytometer. Cells were treated with the half, equal, and double concentrations of the respective IC₅₀ values of the compounds for 24 h.

It is commonly known that Beclin1 is a vital gene involved in the autophagy process. To explore the effect of the compound 10c, the compound was treated at equal and double dose of IC₅₀ values for 24 h,

and then autophagy marker Beclin1 was detected by western blot assay. The result (Fig. 6) showed that autophagy was induced in all those three cancer cell lines after treating with compound 10c compared with

Table 4Cell cycle distribution of K562 cell line treated with **10c** for 24 h.

10c (conc.)	% of cell cycle phases' distribution in K562 cells			
	Sub-G1	G0/G1	S	G2/M
0 nM	1.22%	56.55%	14.65%	27.60%
74 nM	1.78%	51.45%	19.15%	27.70%
148 nM	0.61%	55.10%	15.05%	29.20%
296 nM	0.63%	50.70%	15.75%	32.95%

Table 5Cell cycle distribution of MCF-7 cell line treated with **10c** for 24 h.

10c (conc.)	% of cell cycle phases' distribution in MCF-7 cells			
	Sub-G1	G0/G1	S	G2/M
0 nM	0.69%	40.75%	19.40%	39.40%
53.5 nM	5.89%	52.90%	19.45%	22.90%
107 nM	5.80%	54.85%	20.30%	20.00%
254 nM	2.07%	55.05%	19.05%	24.20%

Table 6Cell cycle distribution of HT29 cell line treated with **10c** for 24 h.

10c (conc.)	% of cell cycle phases' distribution in HT29 cells			
	Sub-G1	G0/G1	S	G2/M
0 nM	0.81%	61.45%	14.65%	23.00%
188 nM	1.74%	62.40%	18.95%	16.93%
376 nM	5.95%	59.55%	21.90%	12.63%
752 nM	2.15%	62.85%	15.10%	19.85%

control.

3.2.3. In vitro kinase screening

The kinase inhibitory activity of the highest potent agent **10c** was detected in order to explore its mechanism of anticancer activity. Compound **10c** was screened at a single dose concentration of 10 μ M over a panel of 21 cancer-associated kinases (Fig. 7). Among the employed kinases, compound **10c** exhibited a significant selectivity towards BRAF^{V600E} and p38 α kinases and inhibited the two kinases by 95% and 86%, respectively. In comparison with the other tested RAF kinases, the mutated BRAF of **10c** significantly superior to its activity over the wild-type BRAF and CRAF, which were inhibited in low percent of 3% and 24%, respectively. It was observed that compound **10c** has moderate activity of 34% against death associated protein kinase 1 (DAPK1), and mild activity of more than 20% over DNA-dependent protein kinase (DNA-PK), epidermal growth factor receptor (EGFR), glycogen synthase kinase-3 β (GSK-3 β), and cyclin-dependent kinases (CDK4/cyclin D1). On the other hand, the inhibition of the remaining panel kinases did not exceed 10%.

3.2.4. In vitro BRAF^{V600E}/p38 α kinase inhibitory activity at 10 μ M

According to the preliminary kinase panel results, all the synthesized derivatives were subjected to BRAF^{V600E} and p38 α inhibitory assay at single dose concentration of 10 μ M in order to identify their dual inhibitory activity (Table 10).

3.2.4.1. Screening of the amide-possessing compounds (7a-d & 10a-d).

The tested compounds showed a wide potency range. Regarding the methoxy derivatives **7a-d**, methyl substitution in **7a** showed moderate activity (46.14%) over BRAF^{V600E} and weak activity (18.11%) against p38 α kinase. Chain elongation in the ethyl derivative **7b** slightly increase the activity of BRAF^{V600E} (52.45%), while the p38 α activity highly improved in more than 4 folds (83.56%). Interestingly, the activity of both kinases declined by substitution with bulkier groups like isopropyl in **7c** and phenyl in **7d**.

Demethylation of **7a-d** to their hydroxyl counterparts **10a-d**,

generally enhanced the activity of all derivatives over the two kinases. The methyl derivative **10a** exhibited the highest inhibition activity of 96.16% and 93.82% against BRAF^{V600E} and p38 α kinases, respectively.

3.2.4.2. Screening of the sulfonamide-possessing compounds (8a,b & 11a, b). Similarly, the methoxy derivatives were evaluated first, the methyl compound **8a** exhibited good activity against BRAF^{V600E} (67.21%) and excellent p38 α activity (95.69%), meanwhile, substitution with the bulky phenyl moiety (**8b**) dramatically decline the BRAF^{V600E} to 9.71% inhibition and reduced the p38 α inhibition activity to 66.59%. However, the hydroxyl derivatives **11a-d** demonstrated significant improvement in BRAF^{V600E} activity to 96.31% and 50.42% inhibition for the methyl (**11a**) and phenyl (**11b**) derivatives, respectively, and slight change in p38 α activity.

3.2.4.3. Screening of the carbamate-possessing compounds (9a-d & 12a-d). Introduction of carbamates at position 2 of the central imidazole ring would have proposed to facilitate the extension into the solvent accessible area. The carbamate functionality participates in additional hydrogen bonding rather than the amides and sulfonamides through the amino acids' carboxyl group and the backbone NH, which in turn improve the molecular stability and pharmacokinetic properties. The carbamate derivatives with methoxy group (**9a-d**) were first screened for BRAF^{V600E} and p38 α activity. The methoxy carbamate compound **9a** exhibited the highest activity over the two kinases (inhibition percentages = 51.79% and 94.81%, respectively), the inhibitory activity was declined for both kinases by substitution with bulkier moieties in compounds **9b**, **9c**, and **9d**. Demethylation into the hydroxyl derivatives **12a-d** improved the BRAF^{V600E} activity two, three, five, four folds in methyl, ethyl, isopropyl, and phenyl derivatives **12a**, **12b**, **12c**, **12d**, respectively. However, no noteworthy changes in p38 α activity were in the hydroxyl derivatives except for the phenyl derivative **12d** which improved by 20% inhibition over its methoxy precursor **9d**.

3.2.5. Potential BRAF^{V600E} and p38 α kinase inhibitory activity (IC₅₀) determination

Among the previously discussed compounds, six compounds (**8a**, **9a, 10a**, **10c**, **12a**, and **12c**), which maintained the highest inhibition over the two kinases (BRAF^{V600E} and p38 α), were subjected to kinase IC₅₀ determination. The inhibitory activity of the selected compounds was measured at 5-dose concentrations (1 nM, 10 nM, 100 nM, 1 μ M, and 10 μ M) in order to determine their IC₅₀ values against both BRAF^{V600E} and p38 α (Table 11). The data indicate that tested compounds exhibited BRAF^{V600E} and p38 α IC₅₀ in low to submicromolar range, except for compound **8a** that exhibited less potent BRAF^{V600E} inhibition with IC₅₀ value > 5 μ M. The overall results exhibited that the tested compounds have higher potency against p38 α over BRAF^{V600E}, except for compound **12a** which is two folds more potent BRAF^{V600E} inhibitor (IC₅₀= 1.62 μ M) than p38 α (IC₅₀= 3.48 μ M). Compounds **10a** and **12c** were emerged to be the highest potent inhibitors with quite equal IC₅₀ values against the two kinases. Compound **9a** is the most potent p38 α inhibitor among the tested compounds. Compound **10c**, the most potent anticancer agent, exhibited distinguishing inhibitory effect on p38 α (IC₅₀= 0.726 μ M) and moderate inhibitory effect on BRAF^{V600E} (IC₅₀= 1.84 μ M).

3.3. Docking study

In order to provide a reasonable explanation of the observed kinase activity and its relation with the characteristic binding interactions of the target compounds, a molecular docking study was conducted in the binding site of both BRAF^{V600E} and p38 α kinases using Molecular Operating Environment (MOE, 2014.0901) software. The two X-ray crystallographic structures of BRAF^{V600E} in complex with GDC0879 (PDB ID: 4MNF) and p38 α kinase in complex with TAK-715 (PDB ID:

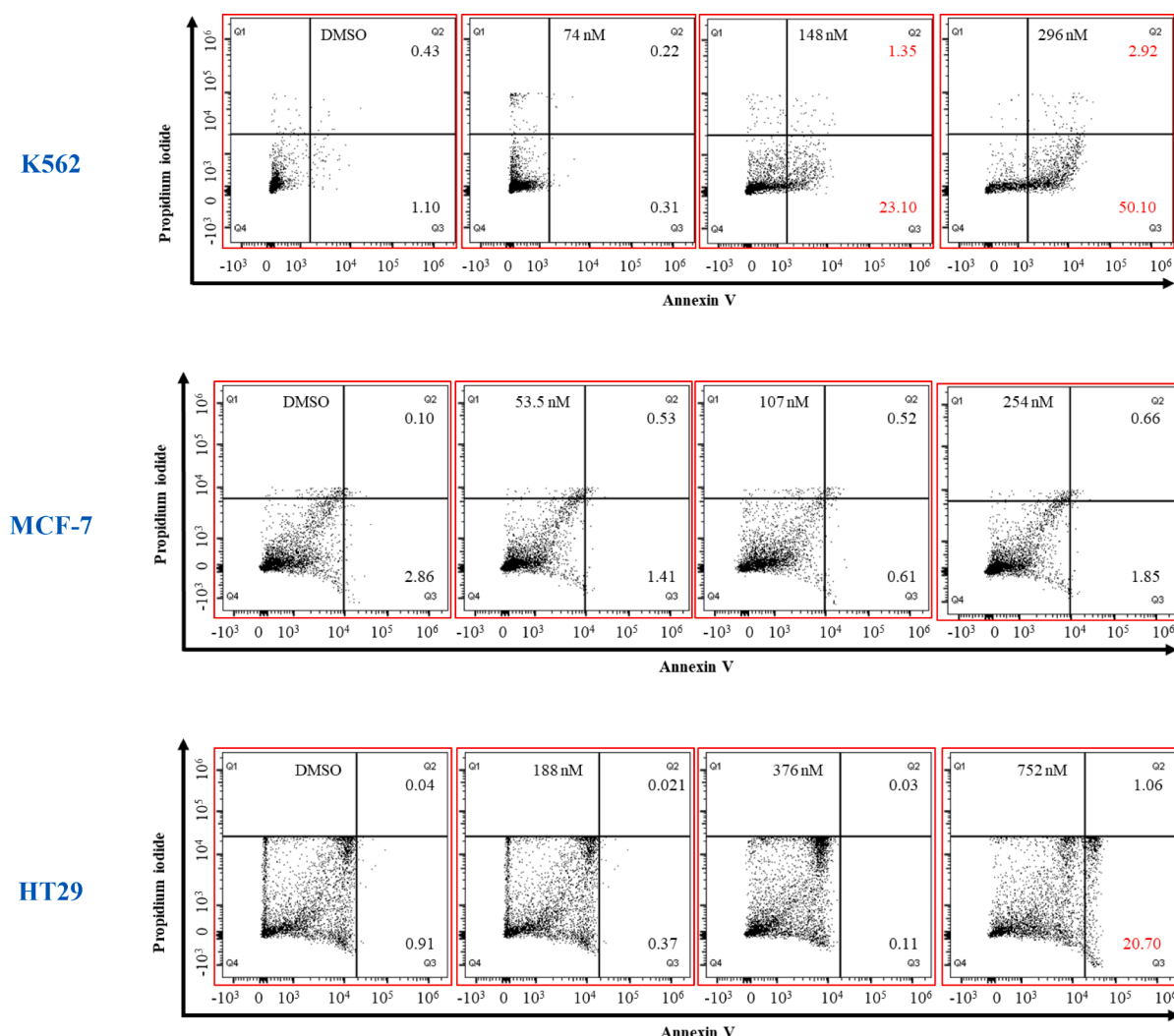


Fig. 5. Characterization of cell apoptosis after treated with compound **10c** for 24 h, as determined by Annexin V and PI staining. Quadrants were defined as Q3 = early-stage apoptosis (Annexin V-positive/PI-negative) and Q2 = late-stage apoptosis (Annexin V-positive/PI-positive). Histogram showed percentages of early apoptotic and late apoptotic cells after 24 h.

Table 7
Apoptotic cell distribution of K562 cell line treated with **10c** for 24 h.

10c (conc.)	% of cell cycle phases' distribution in K562 cells			
	Live	Early apoptosis	Late apoptosis	Necrosis
0 nM	97.85%	1.10%	0.43%	0.64%
74 nM	96.75%	0.31%	0.22%	2.70%
148 nM	73.95%	23.10%	1.35%	1.61%
296 nM	46.55%	50.10%	2.92%	0.42%

Table 8
Apoptotic cell distribution of MCF-7 cell line treated with **10c** for 24 h.

10c (conc.)	% of cell cycle phases' distribution in MCF-7 cells			
	Live	Early apoptosis	Late apoptosis	Necrosis
0 nM	95.65%	2.86%	0.10%	1.39%
53.5 nM	96.15%	1.41%	0.53%	1.90%
107 nM	96.95%	0.61%	0.52%	1.91%
254 nM	96.40%	1.85%	0.66%	1.11%

3ZSG) were downloaded from the Protein Data Bank (PDB) (Azevedo et al., 2012, Haling et al., 2014).

At the beginning, the protocol was validated by re-docking of the co-

Table 9
Apoptotic cell distribution of HT29 cell line treated with **10c** for 24 h.

10c (conc.)	% of cell cycle phases' distribution in HT29 cells			
	Live	Early apoptosis	Late apoptosis	Necrosis
0 nM	97.85%	0.91%	0.04%	1.20%
188 nM	97.55%	0.37%	0.02%	2.05%
376 nM	97.20%	0.11%	0.03%	2.66%
752 nM	77.60%	20.70%	1.06%	0.70%

crystallized ligands, GDC0879 and TAK-715, in the binding sites of BRAF^{V600E} and p38 α , respectively. This revealed the binding pattern of the two kinases (BRAF^{V600E} and p38 α) with their corresponding co-crystallized ligands with energy scores of -7.59 and -9.21 kcal/mol, respectively, and with an RMSD of 0.162 and 0.557 Å, respectively, between the co-crystallized native ligand and the docked poses. The resultant docking poses imitated all the essential molecular interactions possessed by the native ligand in the binding active site of BRAF^{V600E} and p38 α (Table S2, Supplementary File).

As illustrated, BRAF^{V600E} native ligand (GDC0879) anchored in the adenine pocket via H-bond between pyridine nitrogen and Cys532 in the hinge binding area, the hydrophobic pocket was occupied by the oxime moiety on the (Z)-2,3-dihydro-1H-indene, which H-bonded with Glu501

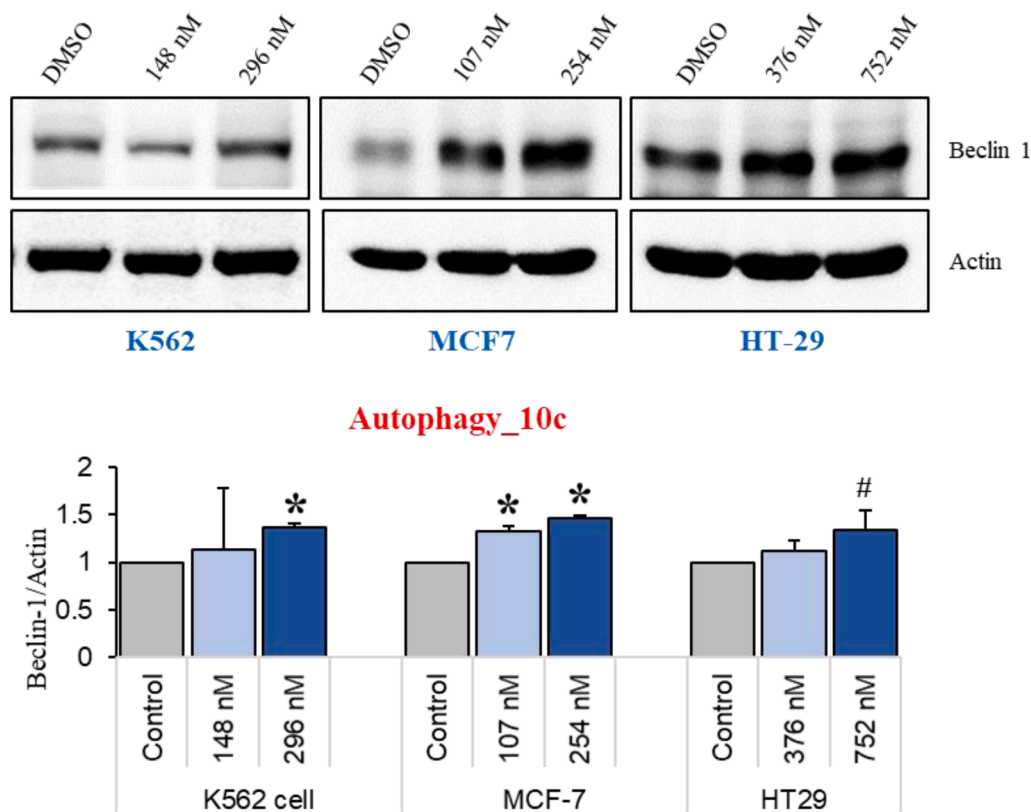


Fig. 6. Autophagic activity in different cells after treated with compound **10c** for 24 h, as determined by western blot using autophagic markers (Beclin1). Bar graphs showed the fold change values of the treated groups compared with control. * $p < 0.05$ and # $p < 0.01$.

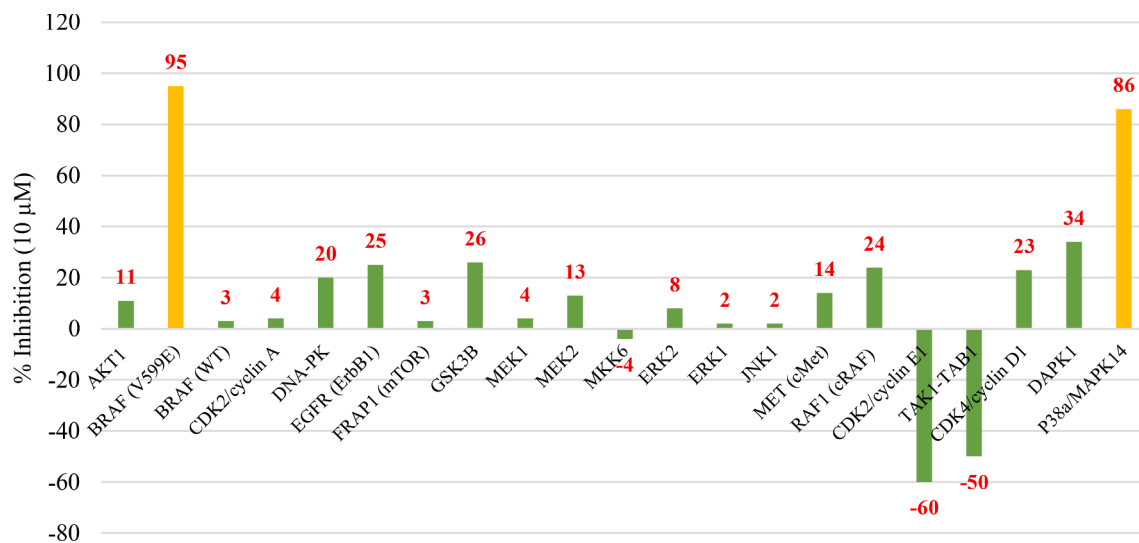


Fig. 7. Inhibition percentages of compound **10c** at 10 μM concentration over a panel of 21 protein kinases.

residue, while the central pyrazole ring was embedded in the ribose pocket through arene-H interaction with Val471, finally, the ligand bound in water accessible area through a H-bond formation with Ser465 by the lateral OH of ethanol moiety (Fig. 8a). However, TAK-715 showed a great affinity to p38α active site. Both pyridine nitrogen and 2-NH₂ pyridine of TAK-715 formed a H-bond with Met109 in the adenine hinge region. The central thiazole ring was deeply buried in the sugar pocket through arene-H interaction with Val38 and Arene-Arene interaction with Phe169 residue, in addition, the thiazole's nitrogen atom formed a h-bond with Lys53 (Fig. 8b).

The enzymatic activity (BRAF^{V600E} and p38α) of the target compounds depends on their ability to properly bind into the active site of both kinases and to establish strong enough interactions with the key amino acids (ligand affinity) in order to compete with the ATP for the binding site. Accordingly, the active compounds in this study should attain the same binding mode observed for the native ligands GDC0879 and TAK-715 (Fig. 8). Analysis of the docking results revealed that the target compounds **7-12** showed quite similar binding interactions in both kinases with predicted docking energy scores in the binding site of both BRAF^{V600E} and p38α kinase ranging from -7.06 to -8.63 kcal/mol

Table 10

Enzyme % inhibition activity of the final target compounds **7a-d**, **8a,b**, **9a-d**, **10a-d**, **11a,b**, and **12a-d** at 10 μ M over BRAF^{V600E} and p38 α kinase^a

Cpd.	kinase % inhibition at 10 μ M		Cpd.	kinase % inhibition at 10 μ M	
	BRAF ^{V600E}	p38 α /MAPK14		BRAF ^{V600E}	p38 α /MAPK14
7a	46.14% \pm 0.78%	18.11% \pm 1.25%	10a	96.15% \pm 0.98%	93.82% \pm 2.07%
7b	52.45% \pm 2.01%	83.56% \pm 0.07%	10b	92.01% \pm 2.32%	73.88% \pm 3.01%
7c	39.76% \pm 1.98%	69.98% \pm 2.08%	10c	95.4% \pm 3.59%	87.24% \pm 0.78%
7d	13.73% \pm 1.02%	39.76% \pm 3.56%	10d	84.99% \pm 2.95%	85.23% \pm 1.63%
8a	67.21% \pm 2.35%	95.69% \pm 1.56%	11a	96.31% \pm 1.08%	99.01% \pm 0.65%
8b	09.71% \pm 1.01%	66.59% \pm 0.45%	11b	50.42% \pm 2.01%	67.62% \pm 2.18%
9a	51.79% \pm 2.52%	94.81% \pm 2.47%	12a	94.87% \pm 2.01%	96.73% \pm 1.13%
9b	34.83% \pm 4.01%	91.21% \pm 2.73%	12b	93.58% \pm 1.63%	89.13% \pm 2.03%
9c	18.62% \pm 0.26%	81.29% \pm 3.20%	12c	96.50% \pm 2.01%	97.79% \pm 3.16%
9d	17.57% \pm 0.28%	59.75% \pm 4.36%	12d	86.21% \pm 2.01%	82.36% \pm 0.68%

^a The results are expressed as means of duplicate assays \pm S.D.

Table 11

IC₅₀ values of the final target compounds **8a**, **9a**, **10a**, **10c**, **12a**, and **12c** over BRAF^{V600E} and p38 α kinases.

Cpd.	BRAF ^{V600E} IC ₅₀ (μ M)	p38 α IC ₅₀ (μ M)
8a	> 5	0.618
9a	ND	0.241
10a	0.530	0.525
10c	1.840	0.726
12a	1.620	3.48
12c	0.542	0.538
GW5074	0.0007	ND
SB202190	ND	0.002

ND: not determined.

and -6.27 to -9.25 kcal/mol, respectively (Table S2). The target molecules exhibited quite typical binding interactions of both GDC0879 and TAK-715. As depicted in Table S2, the central imidazole ring is buried into the ribose pocket of kinase active site via arene-H interaction with Val471 and Val38 of BRAF^{V600E} and p38 α kinase, respectively. Moreover, the hinge binder of the two kinases was occupied by the pyridine moiety, which formed H-bond with Cys532 and Met109 of BRAF^{V600E} and p38 α kinase, respectively exemplified by the binding modes of compounds **10a**, **10c**, **11a**, **11b**, and **12d**. In both kinases, the bromine atom showed a unique halogen interaction, where the bromine acts as a Lewis acid and interacts with the electron donor moiety of Glu501 or Gln530 in BRAF kinase and Leu104 and Ala51 in p38 α . Compounds **10a** and **12c**, with the highest potency against the two kinases, exhibited excellent binding affinity to the ATP active sites of both kinases. In p38 α active site, the central imidazole of the **10a** and **12c** was buried deeply in the ribose pockets through arene-H interaction with Val38 and π - π stacking with Phe169 residues, in addition, their lateral substituted aniline at imidazole's C2 was extended deeply in the phosphate area forming π - π interaction with Tyr35, however, the 2-bromo pyridine moiety of **10a** bound in the hinge binding area was via H-bonding with Met109, the same moiety of **12c** was oriented to the hydrophobic back pocket interacting with Thr106 (Fig. 9).

On the other hand, compounds **10a** and **12c** anchored in BRAF^{V600E} adenine pocket via H-bonding with Cys532 backbone, while the central imidazole ring was directed to the ribose pocket even there is no interaction was detected with Val471 (Fig. 10).

Interestingly, compound **10c**, which demonstrated the highest nanomolar antiproliferative activity even though its kinase activity was moderate (BRAF^{V600E} IC₅₀ = 1.84 μ M & p38 α IC₅₀ = 0.726 μ M), was perfectly fitted in the activity site of the two kinases. As shown in Fig. 11, the central imidazole embedded in the sugar pocket by an arene-H interaction with Val471 and Val38 in the active site of BRAF^{V600E} and p38 α , respectively. The lateral 2-bromopyridine moiety was directed to the hydrophobic pocket of BRAF^{V600E} kinase where the bromine formed a halogen bond with Glu501, however, this moiety anchored in the hinge binder of p38 α via H-bonding with Met109. The terminal 3-hydroxy phenyl moiety represented the hinge binder fragment in BRAF^{V600E} and a H-bond was formed between the OH and Cys532, while this moiety was oriented to the hydrophobic back pocket of p38 α kinase.

3.4. Molecular dynamic simulation

The conducted docking study revealed the high fitting affinity of compound **10c**, the most potent inhibitor, in the active sites of BRAF^{V600E} and p38 α kinases with energy score of -7.75 and -8.69 Kcal/mole, respectively, while the native ligands of the two kinases scored -7.59 and -9.21 kcal/mol, respectively. The characteristic binding of compound **10c** in the two kinases active sites exhibited that **10c** anchored in the hinge binder via H-bonding between the OH group of the 3-hydroxy phenyl moiety and Cys532 of the BRAF^{V600E}, and the nitrogen atom of 2-bromopyridine moiety and Met109 residue of the p38 α kinase, while, the central imidazole of **10c** was deeply buried in the ribose pocket of the two kinases through arene-H interactions with Val471 and Val38 of BRAF^{V600E} and p38 α , respectively.

Accordingly, molecular dynamic (MD) simulation analysis was conducted for compound **10c** in attempt to study the conformational stability of its docked inhibitor-protein complex and to attain dependable drug-receptor binding affinities. MD simulation study was performed for 600 ns for inhibitor **10c** in comparison to the native ligands GDC0879 and TAK-715 in the active sites of BRAF^{V600E} (PDB ID: 4MNF) and p38 α kinase (PDB ID: 3ZSG), respectively. The MD simulations protocol was run at 300 K temperature, and the atomic potential energy was recorded in a time interval of 0.5 ns.

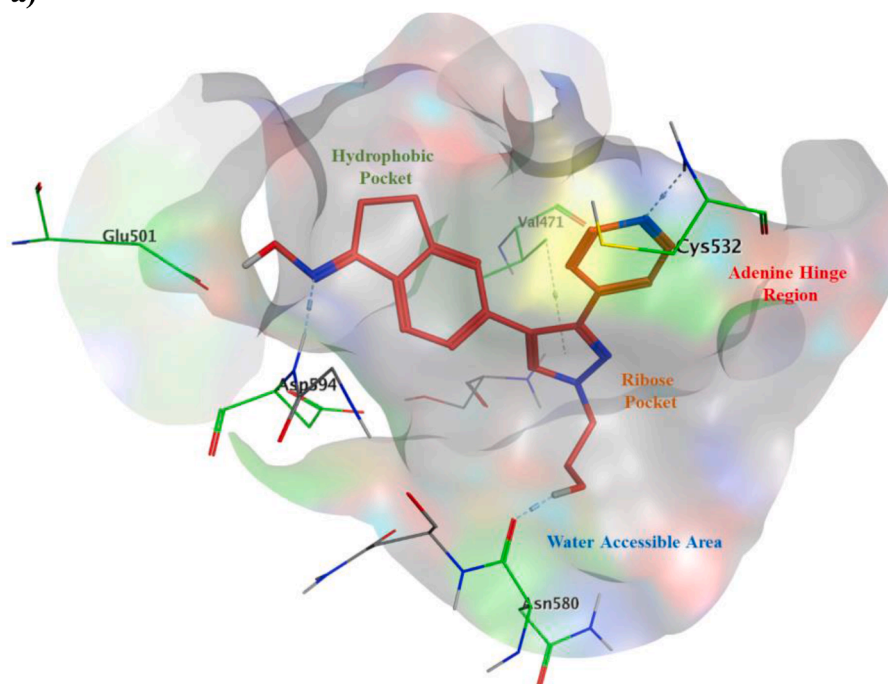
To explore the dynamic stability of both the inhibitor-enzyme complex (4MNF-**10c** and 3ZSG-**10c**) and ligand-enzyme complex (4MNF-GDC0879 and 3ZSG-TAK-715), the time-dependent atomic potential energy of each complex was calculated during MD trajectories. As illustrated in Figs. 12 and 13, the ligand-enzyme complex (4MNF-GDC0879 and 3ZSG-TAK-715) attained the equilibrium around 300 ns and 200 ns, respectively. However, the inhibitor-enzyme complexes (4MNF-**10c** and 3ZSG-**10c**) achieved equilibrium around 250 ns and 200 ns. The obtained results indicate that the native ligand and the tested inhibitor **10c** have retained their binding affinity and kept firmly bound to their respective kinase binding site.

In addition, the root mean square deviation (RMSD) values were observed during the simulation process to predict the stability of the inhibitor-enzyme complex. The recorded RMSD values were also represented as a function of time in Fig. 14. The inhibitor-enzyme complexes exhibited interaction stability during the first 200 ns and 250 ns of the dynamic simulations in the active site of BRAF^{V600E} and p38 α kinases, respectively.

4. Conclusion

This study yielded a series of 4-(imidazol-5-yl)pyridine-based derivatives was designed and synthesized based on a group of structural modifications of previously reported dual BRAF^{V600E}/p38 α inhibitors. The applied structural optimization was aiming at improving the anticancer activity of the new derivatives by enhancing their cell membrane permeability, in addition, boost the molecular affinity in the active site of both BRAF^{V600E} and p38 α kinases via introducing additional hydrophilic moieties in either the solvent accessible area of BRAF^{V600E} kinase

a)



b)

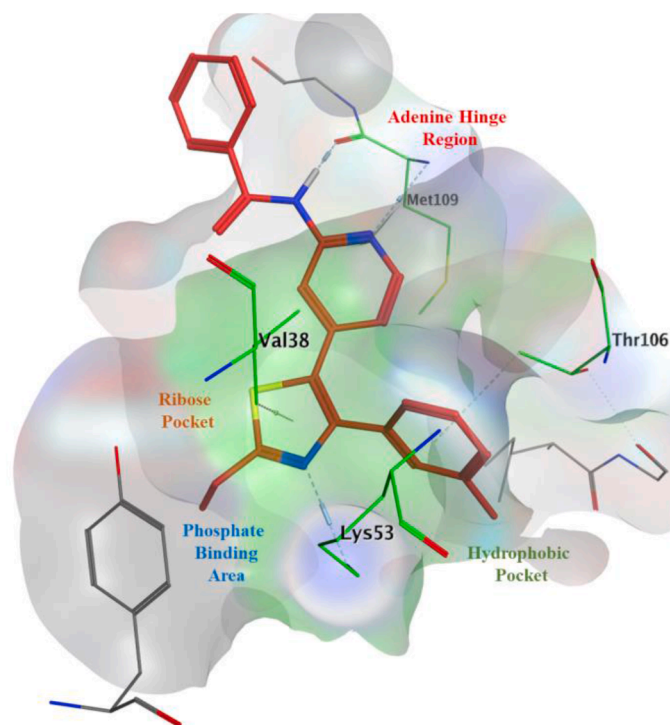


Fig. 8. 3D molecular interaction diagram of: a) GDC0879 in BRAF^{V600E} active site (PDB ID: 4MNF), b) TAK-715 in p38α kinase active site in (PDB ID: 3ZSG).

or the phosphate binding region of p38α kinase. The target compounds showed diversity of amides, sulfonamides, and carbamates substituents, which in turn provide a wide range on biological activities. The synthesized compounds were preliminary screened for their anticancer activity at single dose concentration (10 μM) over a panel of 60-human cancer cell lines. Compounds **7c**, **7d**, **8b**, **9b**, **9c**, **10c**, **10d**, and **11b** exhibited the highest cytotoxic activity over the employed 60-cell lines

generally, leukemia, CNS cancers, renal cancers, and breast cancers with mean % GI = 62% ~ 120%. The active derivatives were selected by NCI for further 5-dose assay to determine their GI₅₀ values. The eight derivatives exhibited a promising activity of sub-micromolar or one-digit micromolar GI₅₀ values against the tested cell lines. Apparently, compound **10c** occurred to be the most potent anticancer agent, which exhibited sub-micromolar activity over the tested 60- cancer cell lines.

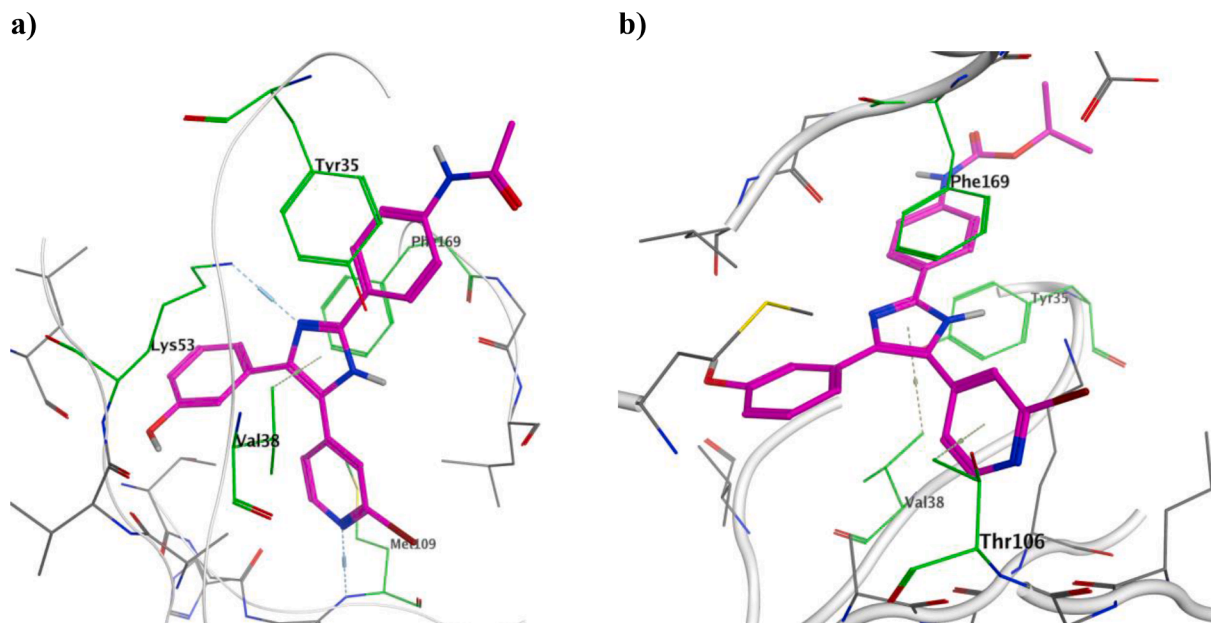


Fig. 9. 3D representation of compound 10a (a) and 12c (b) molecular interactions in the p38 α kinase.

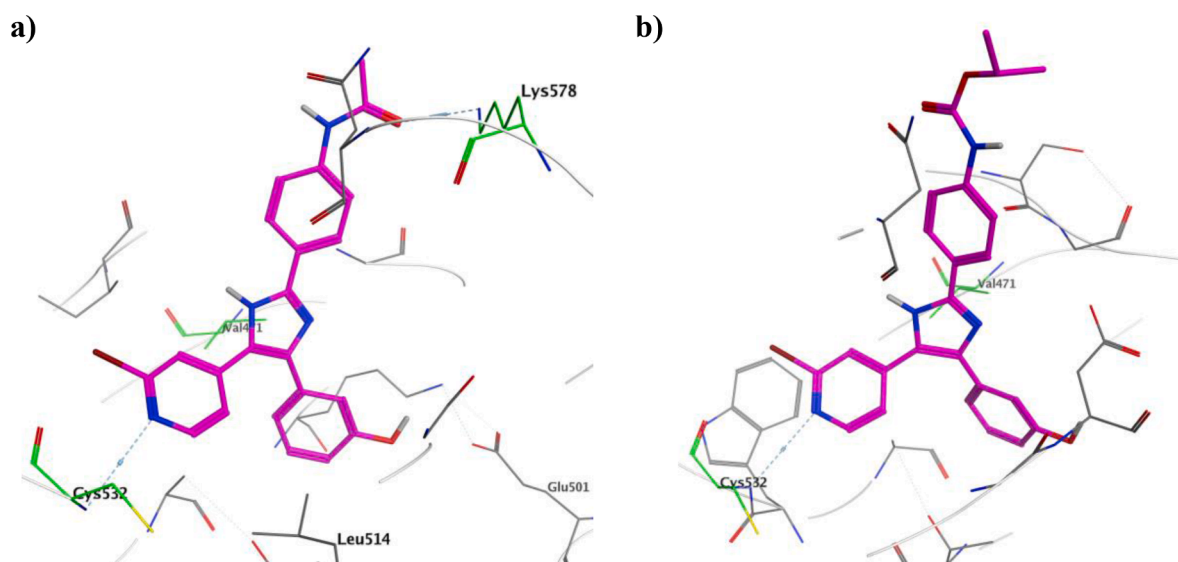


Fig. 10. 3D representation of compound 10a (a) and 12c (b) molecular interactions in the BRAF^{V600E} kinase.

Moreover, compound **10c** showed incredible activity against melanoma (MDA-MB-435) cell line with GI_{50} value of 70 nM. It is extremely more potent than sorafenib against the NCI-60 cell line panel. Additional cell-based mechanistic studies including cell cycle analysis, apoptosis induction, and autophagy analysis were conducted to compound **10c** to explain its possible anticancer mechanism in K562, MCF-7 and HT29 cancer cell lines. Compound **10c** induced cell cycle arrest at G2/M phase in K562 cells, G0-G1 phase in MCF-7 cells and S phase in HT29. Compound **10c** showed a dose-dependent increase in the total, early, and late apoptosis in K562 cells, early apoptotic populations in HT29 cells, no significant apoptosis in MCF-7 cells. The autophagy analysis of revealed that compound **10c** induced autophagy in the three cancer cell lines. Kinase profiling of **10c** showed its inhibitory effects and selectivity towards B-RAF^{V600E} and p38 α kinases. As a result, the target compounds **7a-d**, **8a,b**, **9a-d**, **10a-d**, **11a,b**, and **12a-d** were evaluated for their inhibitory activity against the two kinases. Compounds **10a** and **12c** showed the highest potency against the two kinases. Moreover,

compound **10c**, exhibited inhibitory effect on p38 α (IC_{50} = 0.726 μ M) and moderate inhibitory effect on BRAF^{V600E} (IC_{50} = 1.84 μ M). Molecular modeling studies including molecular docking for the target compounds and molecular dynamic simulations for compound **10c** were conducted in attempt to emphasize the relation between the mentioned kinase inhibitory activity for each derivative and their molecular interaction and stability in the active site of BRAF^{V600E} and p38 α .

Compound **10c** demonstrated high affinity in the kinases pockets. Compound **10c** that possesses terminal isopropyl group, amide linker, and hydroxyphenyl moiety is considered as a promising candidate for developing anticancer agents that could be subjected for further optimization to improve its BRAF^{V600E} and p38 α inhibitory effects.

Supporting information

Supplementary File

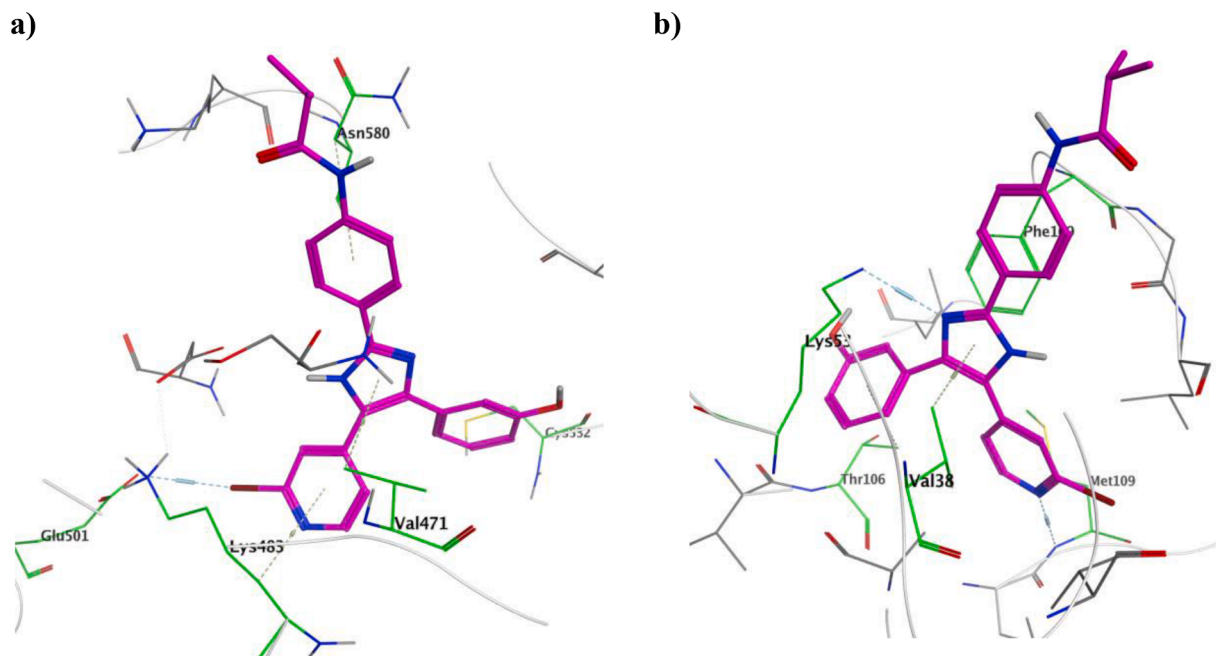


Fig. 11. 3D representation of compound 10c molecular interactions in the active site of BRAF^{V600E} kinase (a) and p38α kinase (b).

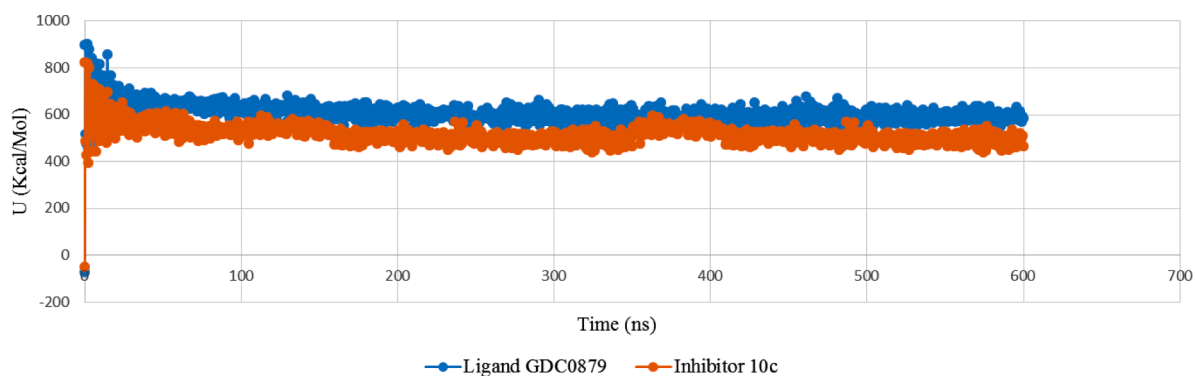


Fig. 12. Potential energy evaluation of complex of compound 10c and native ligand GDC0879 with BRAF^{V600E} kinase (PDB ID: 4MNF) binding site as function of time (ns).

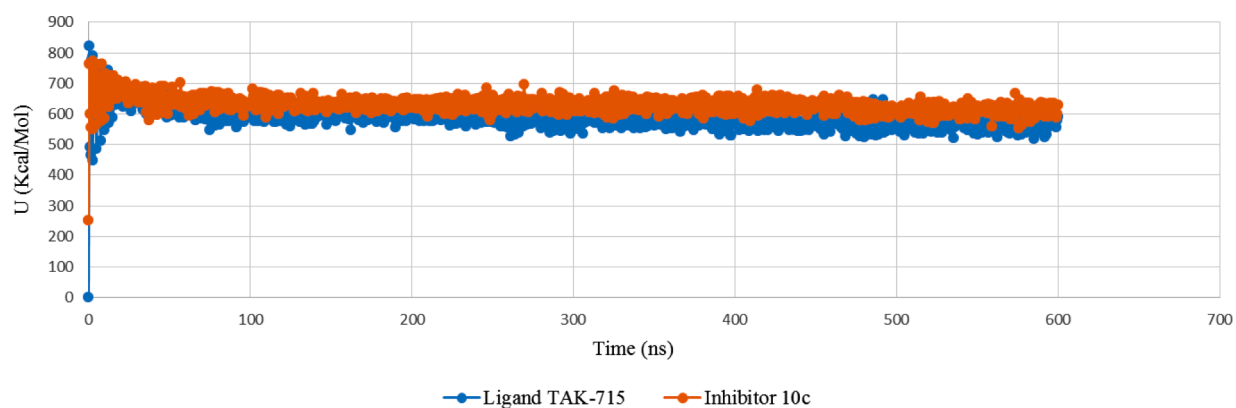


Fig. 13. Potential energy evaluation of complex of compound 10c and native ligand TAK-715 with p38α kinase (PDB ID: 3ZSG) binding site as function of time (ns).

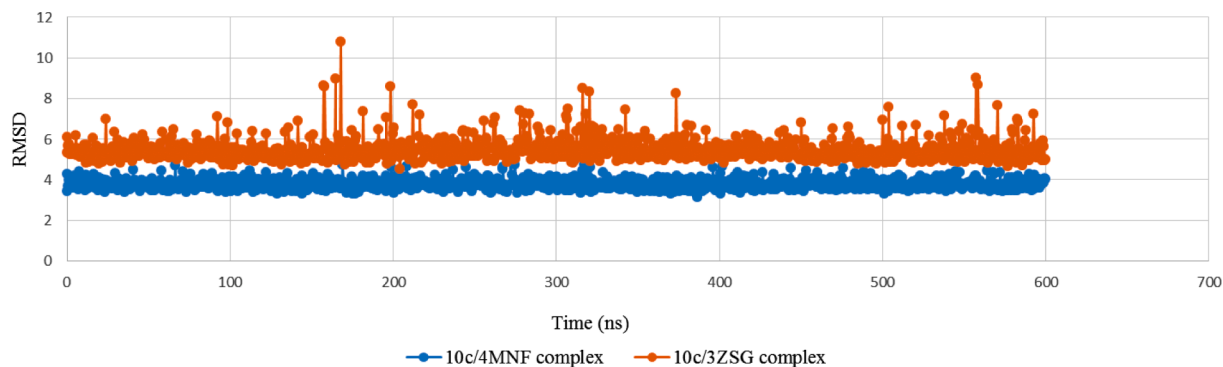
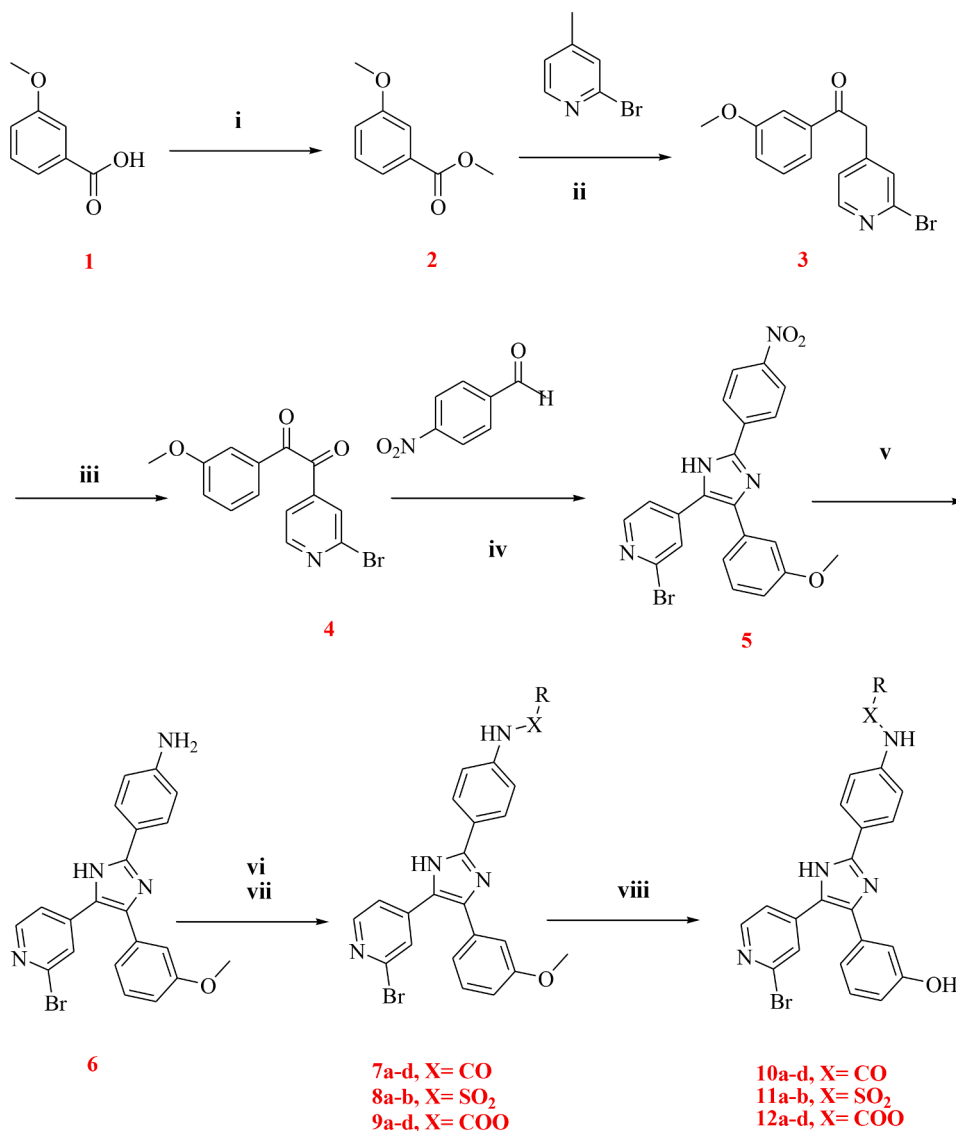


Fig. 14. The RMSD curve from the molecular dynamics simulation of compound **10c** in complex with BRAF^{V600E} kinase (PDB ID: 4MNF) and p38 α kinase (PDB ID: 3ZSG). The x-axis represents the simulation time (ns), while the y-axis represents the RMSD value (nm).



Scheme 1. Reagents and conditions: i) MeOH, conc. H₂SO₄, 80 °C, 12 h.; ii) LiHMDS, THF, -70 °C, 18 h.; iii) HBr, DMSO, 55 °C, 2 h.; iv) NH₄OAc, CH₃COOH, 100 °C, 4 h.; v) SnCl₂•2H₂O, EtOAc, 80 °C, 4 h.; vi) DIPEA, THF, rt, 12 h; vii) THF, 0 °C, N₂, 12 h; viii) BBr₃, DCM, TBAI, -70 °C, 6 h.

Declaration of interest

None.

Acknowledgments

The authors are grateful to Korea Institute of Science and Technology (KIST) (project 2E30341 and 2E31130), National Research Foundation of Korea (NRF) grant funded by the Korea government (MSIT) (NRF-2021R1A2C1011204), the Brain Pool Fellowship Program through the National Research Foundation of Korea (NRF) funded by the Ministry of Science, and ICT (for MMH: NRF-2018H1D3A1A02074556 and for TD: 2017H1D3A1A02054608) for financially supporting this work.

Supplementary materials

Supplementary material associated with this article can be found, in the online version, at doi:[10.1016/j.ejps.2022.106115](https://doi.org/10.1016/j.ejps.2022.106115).

References

- <https://dtp.cancer.gov/>.
 "https://dtp.cancer.gov/discovery_development/nci-60/methodology.htm".
- Ali, E.M., et al., 2021a. "Design, synthesis, and biological evaluation of novel imidazole derivatives possessing terminal sulphonamides as potential BRAFV600E inhibitors." *Bioorganic Chemistry* 106, 104508.
- Ali, E.M., et al., 2021b. "Design, synthesis and anti-inflammatory activity of imidazol-5-yl pyridine derivatives as p38 α /MAPK14 inhibitor." *Bioorganic & Medicinal Chemistry* 31, 115969.
- Ali, E.M., et al., 2021c. Design, synthesis, biological evaluation, and docking studies of novel (imidazol-5-yl) pyrimidine-based derivatives as dual BRAFV600E/p38 α inhibitors. *European Journal of Medicinal Chemistry* 215, 113277.
- Amin, K.M., et al., 2018. Synthesis and molecular docking study of new benzofuran and furo [3, 2-g] chromone-based cytotoxic agents against breast cancer and p38 α MAP kinase inhibitors. *Bioorganic Chemistry* 76, 487–500.
- Anastassiadis, T., et al., 2011. Comprehensive assay of kinase catalytic activity reveals features of kinase inhibitor selectivity. *Nature Biotechnology* 29 (11), 1039–1045.
- Aouadi, M., et al., 2006. Role of MAPKs in development and differentiation: lessons from knockout mice. *Biochimie* 88 (9), 1091–1098.
- Azevedo, R., et al., 2012. X-ray structure of p38 α bound to TAK-715: comparison with three classic inhibitors. *Acta Crystallographica Section D: Biological Crystallography* 68 (8), 1041–1050.
- Bolognesi, M.L., Cavalli, A., 2016. Multitarget drug discovery and polypharmacology. Wiley Online Library.
- Chabner, B.A., Roberts, T.G., 2005. Chemotherapy and the war on cancer. *Nature Reviews Cancer* 5 (1), 65–72.
- Chatterjee, N., Bivona, T.G., 2019. Polytherapy and targeted cancer drug resistance. *Trends in cancer* 5 (3), 170–182.
- Corcoran, R.B., et al., 2010. BRAF gene amplification can promote acquired resistance to MEK inhibitors in cancer cells harboring the BRAF V600E mutation. *Science signaling* 3 (149), ra83–ra84.
- Cuenda, A., Rousseau, S., 2007. p38 MAP-kinases pathway regulation, function and role in human diseases. *Biochimica et Biophysica Acta (BBA)-Molecular Cell Research* 1773 (8), 1358–1375.
- Ding, Z., et al., 2020. Recent advances in isatin hybrids as potential anticancer agents. *Archiv der Pharmazie* 353 (3), 1900367.
- Düzgün, Ş.A., et al., 2017. Differential effects of p38 MAP kinase inhibitors SB203580 and SB202190 on growth and migration of human MDA-MB-231 cancer cell line. *Cytotechnology* 69 (4), 711–724.
- El Rawas, R., et al., 2020. Is p38 MAPK Associated to Drugs of Abuse-Induced Abnormal Behaviors? *International Journal of Molecular Sciences* 21 (14), 4833.
- Garcia-Mayea, Y., et al., 2020. Insights into new mechanisms and models of cancer stem cell multidrug resistance. *Seminars in cancer biology*.
- Haling, J.R., et al., 2014. Structure of the BRAF-MEK complex reveals a kinase activity independent role for BRAF in MAPK signaling. *Cancer cell* 26 (3), 402–413.
- Holderfield, M., et al., 2014. Targeting RAF kinases for cancer therapy: BRAF-mutated melanoma and beyond. *Nature Reviews Cancer* 14 (7), 455–467.
- Kidgera, A. M., et al. (2017). "Dual-specificity phosphatase 5 controls the localized inhibition, propagation, and transforming potential of ERK signaling.
- Krishnan, K.G., et al., 2020. Novel cyanoacetamide integrated phenothiazines: Synthesis, characterization, computational studies and in vitro antioxidant and anticancer evaluations. *Journal of Molecular Structure* 1199, 127037.
- Mathers, C.D., 2020. History of global burden of disease assessment at the World Health Organization. *Archives of Public Health* 78 (1), 1–13.
- Ono, K., Han, J., 2000. The p38 signal transduction pathway activation and function. *Cellular signalling* 12 (1), 1–13.
- Prahalad, A., et al., 2012. Unresponsiveness of colon cancer to BRAF (V600E) inhibition through feedback activation of EGFR. *Nature* 483 (7387), 100–103.
- Roskoski Jr., R., 2019. Targeting ERK1/2 protein-serine/threonine kinases in human cancers. *Pharmacological research* 142, 151–168.
- Shchemelinin, I., et al., 2006. Protein kinases, their function and implication in cancer and other diseases. *Folia biologica* 52 (3), 81.
- Tiacci, E., et al., 2011. BRAF mutations in hairy-cell leukemia. *New England Journal of Medicine* 364 (24), 2305–2315.
- Wada, T., Penninger, J.M., 2004. Mitogen-activated protein kinases in apoptosis regulation. *Oncogene* 23 (16), 2838–2849.
- Wan, Y., et al., 2019. Indole: A privileged scaffold for the design of anti-cancer agents. *European journal of medicinal chemistry* 183, 111691.
- Zhang, J., et al., 2019. Tetrazole hybrids with potential anticancer activity. *European journal of medicinal chemistry* 178, 341–351.
- Zhang, Y., Dong, C., 2007. Regulatory mechanisms of mitogen-activated kinase signaling. *Cellular and molecular life sciences* 64 (21), 2771–2789.